Bioorganic & Medicinal Chemistry 27 (2019) 4013–4029

Contents lists available at ScienceDirect

Bioorganic & Medicinal Chemistry

journal homepage: www.elsevier.com/locate/bmc

Alkynamide phthalazinones as a new class of TbrPDEB1 inhibitors (Part 2)

Erik de Heuvel[a], Abhimanyu K. Singh[b,f], Pierre Boronat[a], Albert J. Kooistra[a], Tiffany van der Meer[a], Payman Sadek[a], Antoni R. Blaazer[a], Nathan C. Shaner[d], Daphne S. Bindels[e], Guy Caljon[c], Louis Maes[c], Geert Jan Sterk[a], Marco Siderius[a], Michael Oberholzer[e], Iwan J.P. de Esch[a], David G. Brown[b], Rob Leurs[a,*]

[a] Division of Medicinal Chemistry, Amsterdam Institute for Molecules, Medicines and Systems, Vrije Universiteit Amsterdam, 1081 HZ Amsterdam, The Netherlands
[b] School of Biosciences, University of Kent, Canterbury CT2 7NJ, UK
[c] Laboratory for Microbiology, Parasitology and Hygiene, University of Antwerp, 2610 Wilrijk, Belgium
[d] University of California, San Diego, School of Medicine, Department of Neuroscience, 9500 Gilman Drive La Jolla, CA 92093-0662, USA
[e] Scintillon Institute, 6868 Nancy Ridge Drive, San Diego CA-92117, USA

ARTICLE INFO

Keywords:
Trypanosoma brucei phosphodiesterase B1
Enzyme inhibitors
Neglected tropical disease
Human African trypanosomiasis
Structure-based drug discovery
Fluorescence microscopy

ABSTRACT

Inhibitors against *Trypanosoma brucei* phosphodiesterase B1 (TbrPDEB1) and B2 (TbrPDEB2) have gained interest as new treatments for human African trypanosomiasis. The recently reported alkynamide tetrahydrophthalazinones, which show submicromolar activities against TbrPDEB1 and anti-*T. brucei* activity, have been used as starting point for the discovery of new TbrPDEB1 inhibitors. Structure-based design indicated that the alkynamide-nitrogen atom can be readily decorated, leading to the discovery of **37**, a potent TbrPDEB1 inhibitor with submicromolar activities against *T. brucei* parasites. Furthermore, **37** is more potent against TbrPDEB1 than hPDE4 and shows no cytotoxicity on human MRC-5 cells. The crystal structures of the catalytic domain of TbrPDEB1 co-crystalized with several different alkynamides show a bidentate interaction with key-residue Gln874, but no interaction with the parasite-specific P-pocket, despite being (uniquely) a more potent inhibitor for the parasite PDE. Incubation of blood stream form trypanosomes by **37** increases intracellular cAMP levels and results in the distortion of the cell cycle and cell death, validating phosphodiesterase inhibition as mode of action.

1. Introduction

The two causative agents of human African trypanosomiasis (HAT), i.e. *Trypanosoma brucei* (*T.b.*) *rhodesiense* and *T.b. gambiense* are endemic in sub-Saharan Africa.[1,2] The drugs against HAT currently available on the market have major disadvantages, including limited clinical efficacy in certain disease stages, complex administration protocols and toxicity.[1,3–5] Additionally, the small repertoire of available drugs against HAT suffers from emerging drug resistance.[6–10] While the number of new HAT cases has dropped considerably in the last few years,[11] there remains an interest in developing novel and non-toxic trypanocidal agents.[6–10] Several enzymes have been identified as potential targets for development of such new treatments.[12–16] For example, *T. brucei* 3′5′-cyclic nucleotide phosphodiesterase B1 and B2 (TbrPDEB1 and TbrPDEB2) have been validated as essential enzymes of the parasite and can be exploited as a drug target.[16,17] The high sequence homology (88%) between the catalytic sites of the TbrPDEB1 and B2 creates a high degree of equipotency against the paralogues.[17–19] However, selectivity for the parasite PDE over the human orthologues, especially human PDE4 (hPDE4), is required to limit unwanted side effects (*e.g.* emesis, gastrointestinal disturbance and immune suppression).[19–23]

Over the years, several studies reported different hPDE4 inhibitors as starting point for TbrPDEB1 inhibitors, resulting in a number of potent inhibitors, *e.g.* cilomilast analogue **2** and rolipram analogue **4** (Fig. 1).[19,24] However, selectivity for TbrPDEB1 over hPDE4 in combination with antiparasitic activity has been a challenge.[19,24]

Recently, we have shown that the activity profile for TbrPDEB1 over hPDE4 can be obtained by targeting a parasite-specific P-pocket present near the active site of TbrPDEB1.[25,26] Biphenyl tetrahydrophthalazinone NPD-008 (**5**) (Fig. 2) exhibits a submicromolar potency for TbrPDEB1 (pK_i = 7.0) and a 10-fold selectivity over hPDE4 (pK_i = 6.0).[25] The crystal structure of **5** (PDB: 5G2B) in the catalytic

* Corresponding author.
E-mail address: r.leurs@vu.nl (R. Leurs).
[f] Present address: Rega Institute for Medical Research, KU Leuven, 3000 Leuven, Belgium.

https://doi.org/10.1016/j.bmc.2019.06.026
Received 11 May 2019; Received in revised form 12 June 2019; Accepted 14 June 2019
Available online 05 July 2019

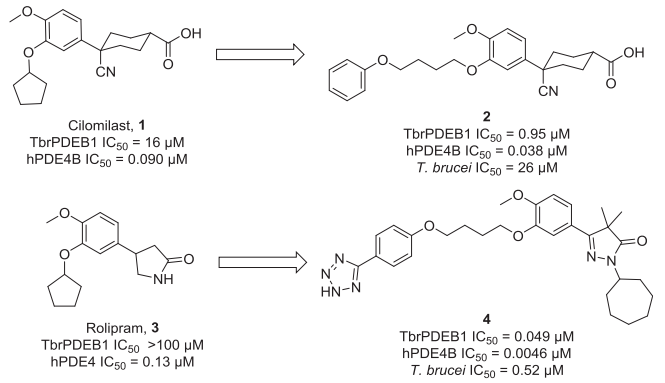

Fig. 1. Repurposing hPDE4 inhibitors for the development of potent TbrPDEB1 inhibitors for the treatment of human African trypanosomiasis.[19,24]

domain of TbrPDEB1 shows that the glycinamide tail occupies the P-pocket thereby explaining the observed selectivity for TbrPDEB1 over hPDE4 (Fig. 2).[25] Successful targeting of the P-pocket was also observed in the crystal structure of TbrPDEB1 co-crystallized with NPD-937 (**6**, PDB: 5L8Y), indicating that a longer and more spacious tail group is also able to enter the P-pocket resulting in selectivity for TbrPDEB1 over hPDE4 (TbrPDEB1 pK_i = 6.4 *vs* hPDE4 pK_i = 5.5).[25] However, **5** and **6** show an unfortunate reduced phenotypic activity against *T. brucei* (pIC_{50} = 5.3 and pIC_{50} = 5.1, respectively), thereby halting further development of these compounds as trypanocidals.[25] Further research to replace the phenyl linker and tail group of **5** by an alkynamide resulted in the discovery of NPD-048 (**7**) which displays a submicromolar potency against TbrPDEB1 (TbrPDEB1 pK_i = 6.2).[27] Although this alkynamide does not show a similar activity profile (hPDE4 pK_i = 6.5) as observed with **5**, the phenotypic activity against *T. brucei* (pIC_{50} = 6.0) improved considerably compared with **5**. Moreover, the co-crystal structure of **7** (PDB: 6FTM) in the catalytic domain of TbrPDEB1 indicates that the scaffold forms a good bidentate interaction with the conserved glutamine residue Gln874 while the alkynamide nitrogen atom offers a promising vector to grow the compound towards the P-pocket.[27]

Herein, we report the structure-based design of new alkynamide tetrahydrophthalazinones with different amide substituents in an attempt to obtain ligands with a better antiparasitic activity.

2. Results and discussion

2.1. In silico exploration of the amide vector

The crystal structures of TbrPDEB1 ligated with **5**, **6** and **7** (PDB-codes 5G2B, 5L8Y, and 6FTM respectively)[25,27] were used to explore suitable amines to decorate the scaffold of **7** to fit the vector towards the P-pocket described by the alkynamide. All three crystal structures were used as basis because the P-pocket volume varies, indicating the flexibility of the P-pocket residues. Reaxys was used to extract all commercially available (eMolecules) primary or secondary amines with a molecular mass below 158 Da. Using the *combinatorial library module* of Molecular Operating Environment (MOE) software package of Chemical Computing Group, the amines were virtually coupled to the alkyne tetrahydrophthalazinone scaffold to make a combinatorial library consisting of 16,153 substituted alkynamides. These molecules were docked using PLANTS[28] into each of the three aforementioned TbrPDEB1 structures and all resulting docking poses were scored using Interaction Fingerprints[29] (IFP) for the core scaffold of the molecules. After applying combined scoring cut-offs[30] (PLANTS ≤ -90 and IFP ≥ 0.5) and filtering for binding poses in which the ligand was in contact with Gln874, there were 2291 unique molecules left. The docking results of the 3 different crystal structures were compared and the overlapping hits were visually inspected (see Fig. 3A). Six compounds, consisting of aliphatic and aromatic substitutions of variating complexity, were hits in all three sets of docking results (Fig. 3B). Compounds with a second (primary or secondary) amine or additional chiral centre were removed from the results to increase synthetic feasibility and to eliminate compounds with more than two diastereomers, nominating only **11** and **12** for synthesis. Non-chiral amines that were hits in two of the three sets of docking results (88 compounds) contained a higher abundancy of aromatic tail groups (66%) versus aliphatic tail groups (33%), thereby predicting a better occupancy of the P-pocket by aromatic groups than aliphatic groups. Most amines contained a second heteroatom that can function as a hydrogen bond acceptor, but no clear preference for flexible or (ring) strained amines was observed. These results were used as inspiration for the compounds synthesized from readily available amines.

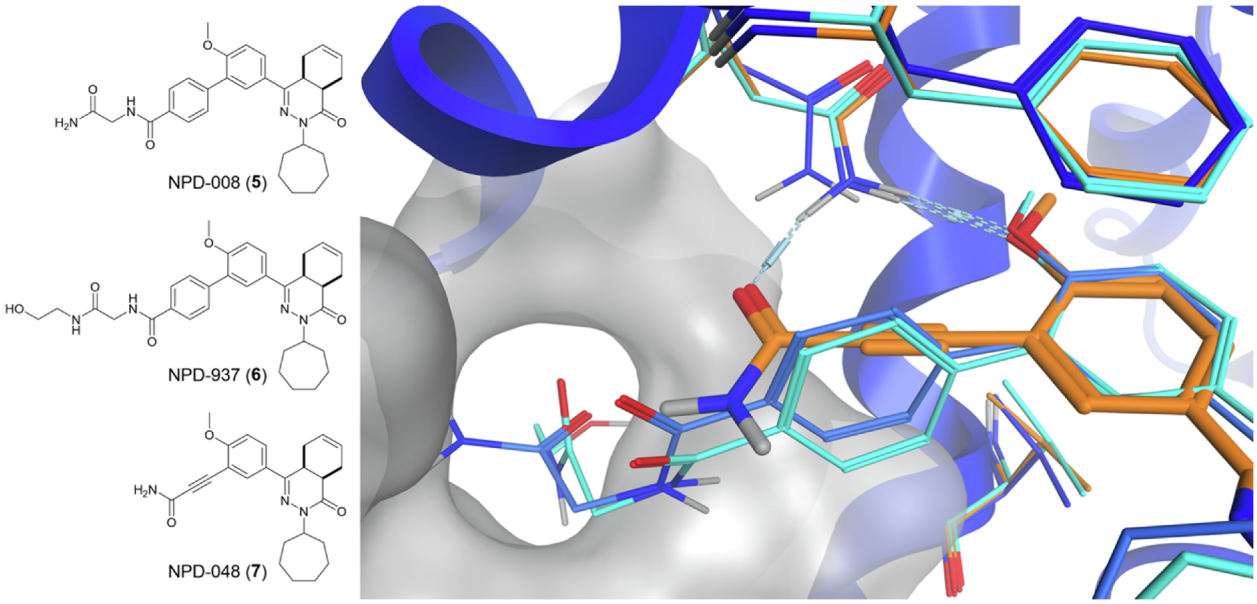

Fig. 2. The structures of the reported tetrahydrophthalazinone-based TbrPDEB1 inhibitors with a phenylamide (**5** and **6**) or alkynamide linker (**7**) and their binding pose in the catalytic domain of TbrPDEB1. Key active site residues and the P-pocket are shown for clarity. NPD-008 (**5**) is displayed in blue, NPD-937 (**6**) in cyan and NPD-048 (**7**) in orange.

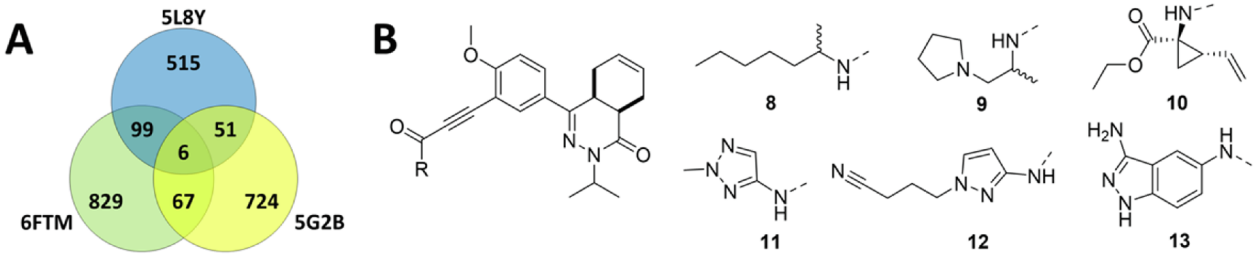

Fig. 3. Virtual screening results. A) Number of hits of the docking in different TbrPDEB1 crystal structures indicated by PDB-code. B) Structures of the 6 amines found in all three databases.

2.2. Chemistry

The previously reported synthetic pathway towards phthalazinone alkynamides contained several steps with low yield and long reaction times.[25,27] Revision of these steps resulted in the design of a new synthetic route (Scheme 1) with reduced reaction times, easier purifications and improved yields. In this new scheme 2-bromoanisole was used in a Friedel-Craft acylation with maleic anhydride to obtain carboxylic acid **14** in good yield. The conversion towards the *E*-isomer was also reported by Onoue *et al.*[31] and confirmed by NMR based on the ^3J-coupling constant of 15.4 Hz between the vinylic hydrogens, typical for *trans* alkene protons. The cyclohexene moiety was introduced by a Diels-Alder reaction with butadiene to form carboxylic acid **15** in quantitative yield. The subsequent condensation with hydrazine and alkylation with isopropylbromide was performed as reported previously.[25,27] It was decided to install an isopropyl group instead of a cycloheptyl substituent of the phthalazinone scaffold for this series of alkynamides, as this modification has been shown to yield a small positive effect on the activity profile.[25,27] Conversion of the stereochemical configuration from the *trans*-cyclohexene to the *cis*-cyclohexene occurs under strongly basic conditions. Comparison of the NMR-spectra of *trans*-tetrahydrophthalazinone **16** with the *cis*-tetrahydrophthalazinone synthesized according to previous reported methods[25] showed distinct differences in shift of aromatic protons (spectra in Supporting Info).

Alkylation of **16** with excess of sodium hydride resulted in a fast conversion towards the *cis*-tetrahydrophthalazinone, which was confirmed by nuclear magnetic resonance (NMR) spectroscopy using Nuclear Overhauser Enhancement (NOE) experiments. Upon saturation of the signal of proton H4a in **15** and **16**, a weak NOE correlation with H8a was observed in the NOE difference spectrum. Saturation of the signal of proton H4a in **17** resulted in a strong NOE correlation with H8a and thereby confirming the *cis*-configuration of **17** (spectra in Supporting Info). Furthermore, the observed ^3J-values of H4a are in agreement with the *trans*-isomer for **16** with one small and two large coupling constants (^3J = 14.6, 11.4 and 5.4 Hz), indicating one axial-equatorial and two axial-axial positioned protons.[32] The opposite was observed for *cis*-isomer **17** with one larger and two smaller coupling constants (^3J = 11.5 and 2 × 5.8 Hz) as a result of one axial-axial coupling and two axial-equatorial protons. The alkyne functionality was introduced using combined Sonogashira/Hiyama reaction conditions with TMS-protected triethylorthopropiolate **18**, which was synthesized in a Grignard reaction from TMS-acetylene in high yield, to obtain ethyl ester **19**. The various amides were obtained by coupling the corresponding amines to ester **19** using $AlMe_3$ in DCM.

2.3. PDE-activity assay

The PDE-activity on TbrPDEB1 and hPDE4 of the synthesized alkynamides was measured to assess their potency and selectivity as TbrPDEB1 inhibitors. Aliphatic alkynamides **20–27** showed comparable submicromolar potencies against TbrPDEB1 in a pK_i range of 6.0 to 6.5

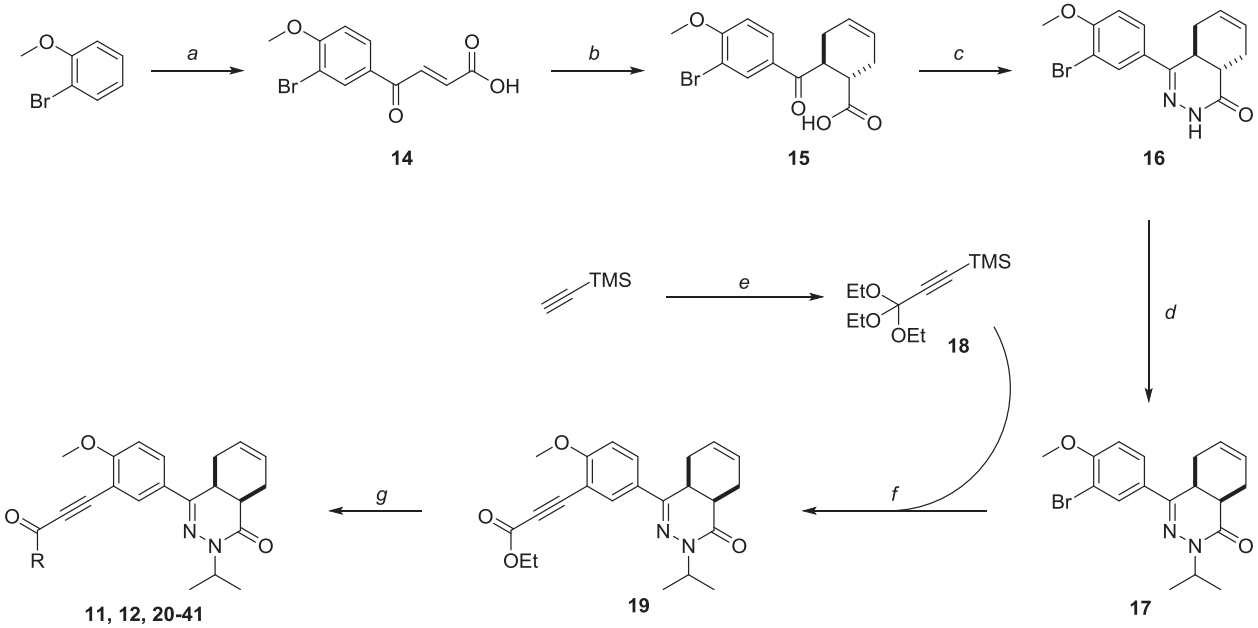

Scheme 1. Reagents and conditions: *a*) maleic anhydride, $AlCl_3$, DCM, rt, overnight, 66%; *b*) 13% butadiene in THF, 140 °C (MW), 30 min, 97%; *c*) $N_2H_4{\cdot}H_2O$, EtOH, reflux, 4 h, 86%; *d*) 1) NaH, DMF, rt, 30 min, 2) isopropylbromide, DMF, rt, 4 h, 81%; *e*) 1) *i*PrMgBr, Et_2O, 10 °C, 30 min; 2) tetraethoxymethane, Et_2O, rt, 1 h, 93%; *f*) $PdCl_2$(dppf), CuI, CsF, Et_3N, DMF, 120 °C (MW), 4 h, 70%; *g*) corresponding amine, K_2CO_3, $AlMe_3$, (Et_3N for HCl-salts), DCM, rt, overnight, 9–84%

Table 1
Structure-activity relationship of alkynamides with aliphatic tail groups for TbrPDEB1 and hPDE4.

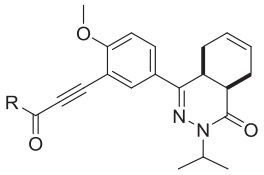

			pK_i (mean ± S.E.M.)[a]					pK_i (mean ± S.E.M.)[a]	
#	NPD	R	TbrPDEB1	hPDE4	#	NPD	R	TbrPDEB1	hPDE4
20	1170		6.3 ± 0.05	6.5 ± 0.1	**24**	1167	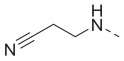	6.0 ± 0.1	6.1 ± 0.1
21	1024	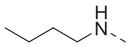	6.5 ± 0.04	6.3 ± 0.1	**25**	1041	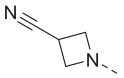	6.2 ± 0.1	6.4 ± 0.1
22	1038	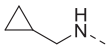	6.4 ± 0.1	6.5 ± 0.1	**26**	1043	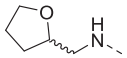	6.4 ± 0.1	5.9 ± 0.2
23	1042	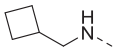	6.5 ± 0.1	6.1 ± 0.1	**27**	1336	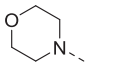	6.0 ± 0.1	6.1 ± 0.1

[a] Mean and S.E.M. values of at least 3 independent experiments.

(Table 1). Most alkynamides showed similar or lower potency for hPDE4 compared to TbrPDEB1, with the best selectivity index (SI, TbrPDEB1 pK_i – hPDE4 pK_i) observed for the tetrahydrofuranyl-substituted analogue **26** (SI = 0.5).

The alkynamides that contain aromatic rings in the tail group (**11**, **12** and **28–41**, Table 2) showed in general higher potencies for TbrPDEB1 (pK_i range 6.1–7.0) when compared to the aliphatic alkynamides. Interestingly, both compounds that were directly selected from the virtual screening (**11** and **12**) showed the lowest potency on TbrPDEB1 observed for the aromatic series of alkynamides. There was no difference observed between a furan and thiophene ring (**28** and **30**), both having a nanomolar potency against TbrPDEB1 (pK_i = 6.9).

Introducing a methyl group on the furan (**29**) or elongating the tail group for the thiophene (**31**) slightly reduced the potency for TbrPDEB1. Implementing a thiazole ring (**32–34**) in the tail group did not improve the potency or selectivity of the alkynamides. Methylpyrrole **35** was equally potent against TbrPDEB1 as 2-methylfuran **28** and 2-methylthiophene **30**, but with a slightly better SI (Table 2, SI = 0.7). Imidazole **36** with a more flexible tail displayed a reduced activity and selectivity.

The highest potencies were observed for pyridinyl alkynamides **38** (NPD-1169, pK_i = 7.0) and **39** (NPD-1334, pK_i = 7.0), which were slightly more potent than the benzyl analogue **37** (pK_i = 6.8), while the less flexible 3-methoxyphenyl analogue **40** displayed a pK_i of 6.7 against TbrPDEB1. Fluorophenyl **41** showed a slightly reduced potency and selectivity when compared with benzyl analogue **37**.

When compared to the previously synthesized primary alkynamide **7** with a SI of −0.3 (Fig. 4), most compounds (except **11**) show a slightly improved selectivity index for TbrPDEB1 over hPDE4 and several compounds display a comparable selectivity to **5** (SI = 1.0). The SI observed for **39** was 0.8 log unit, making this 4-pyridinyl alkynamide approximately 6-times more potent against TbrPDEB1 than hPDE4.

2.4. Co-crystal structures in TbrPDEB1 and hPDE4

We successfully obtained co-crystal structures of **37**, **40** and **41** (PDB: 6GXQ, 6RFN and 6RFW, respectively, Fig. 5) and the previously reported NPD-053 (**42**) and NPD-055 (**43**) (PDB: 6RB6 and 6RGK, respectively) in the catalytic domain of TbrPDEB1 and co-crystal structures of **37** and **42** bound in the catalytic domain of hPDE4 (PDB: 6HWO and 6RCW respectively). While our design indicated that decoration of the alkynamide nitrogen of **7** is possible in TbrPDEB1 because of the presence of the parasite-specific P-pocket, the crystal structures of **37** show that the amide substituent does not occupy the P-pocket (Fig. 5A).

While a bidentate interaction with the key Gln874 of TbrPDEB1 is maintained, the amide substituent folds back in a hydrophobic collapse. A highly similar binding pose is observed in the co-crystal structure of **37** in hPDE4 (Fig. 5B). The comparison of the co-crystal structures of **42** in hPDE4 and TbrPDEB1 gave a similar result (See Supporting Info). While the ligands do not seem to exploit the parasite-specific P-pocket, the crystal structures do not give an explanation for the improved activity profile for TbrPDEB1 over hPDE4. The tail groups seem to fold back towards Phe877 of the hydrophobic clamp, but no substantial additional interactions are observed. In addition, an overlay of the binding poses of **37**, **40**, **41**, **42** and **43** in the catalytic domain of TbrPDEB1 (Fig. 5C) shows that they occupy the same space in the binding site (images of individual crystal structures can be found in the Supporting Info).

2.5. Surface plasmon resonance biosensor analysis

To increase our understanding of ligand-PDE binding and the molecular features that have an influence on the resulting activity profiles, we performed interaction analyses using a surface plasmon resonance (SPR) biosensor assay (Fig. 6). Biotinylated proteins were captured by neutravidin, immobilized on CM5 chip surface. Interaction assays were performed by injecting suitable concentration series for each compound. Compounds **20** and **37** were injected for respectively 60 and 320 s to reach steady-state equilibrium and their dissociation was monitored (300 s for **20** and 900 s for **37**) to determine the pK_D values. The affinity of the unsubstituted alkynamide **20** at hPDE4D (pK_D = 6.6 ± 0.1) was ~0.5 log unit higher compared to the affinity obtained for its binding to TbrPDEB1 (pK_D = 6.1 ± 0.1). Going from **20** to the benzyl substituted analog **37**, the affinity for TbrPDEB1 (pK_D = 7.1 ± 0.1) improved 10-fold, while at hPDE4D (pK_D = 7.1 ± 0.1) the affinity of **37** was only 0.5 log-unit higher. These findings indicate that the benzyl substitution of the alkynamide has a pronounced effect on TbrPDEB1 binding, as **37** is equipotent at TbrPDEB1 and hPDE4. Interestingly, while the obtained crystal structures do not easily explain the improved biochemical activity profile of

Table 2
Structure-activity relationship of alkynamides with aromatic tail groups.

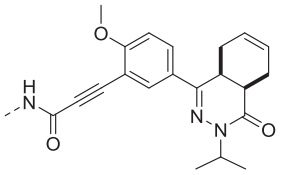

#	NPD	R	pK_i ± S.E.M.[a] TbrPDEB1	hPDE4	#	NPD	R	pK_i ± S.E.M.[a] TbrPDEB1	hPDE4
11	3154	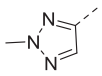	5.6 ± 0.1[b]	6.3 ± 0.1	**34**	3153	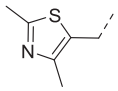	6.7 ± 0.01	6.6 ± 0.3
12	3155	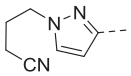	6.1 ± 0.02	5.9 ± 0.2	**35**	1321	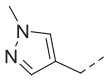	6.9 ± 0.1	6.2 ± 0.1
28	1016	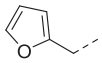	6.9 ± 0.04	6.4 ± 0.1	**36**	1323	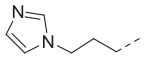	6.4 ± 0.03	6.2 ± 0.2
29	1174	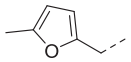	6.7 ± 0.2	6.7 ± 0.1	**37**	1335	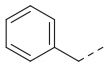	6.8 ± 0.1	6.1 ± 0.2
30	1322	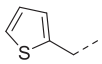	6.9 ± 0.04	6.3 ± 0.1	**38**	1169	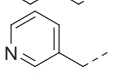	7.0 ± 0.1	6.3 ± 0.1
31	1320	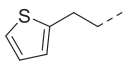	6.4 ± 0.01	6.1 ± 0.1	**39**	1334	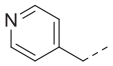	7.0 ± 0.1	6.2 ± 0.1
32	1171	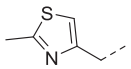	6.5 ± 0.1	6.0 ± 0.1	**40**	1018	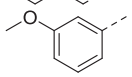	6.7 ± 0.1	6.0 ± 0.1
33	1319	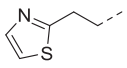	6.6 ± 0.1	6.4 ± 0.2	**41**	1039	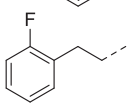	6.5 ± 0.1	6.1 ± 0.1

[a] Mean and S.E.M. values of at least 3 independent experiments.

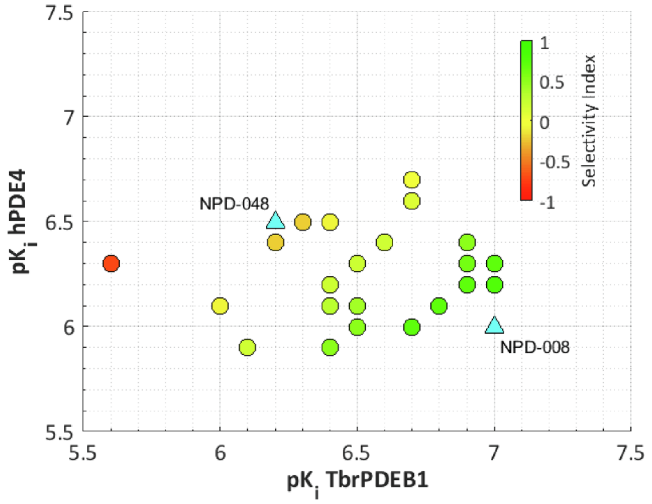

Fig. 4. Biochemical activity against TbrPDEB1 and hPDE4 of all alkynamides and reference compounds NPD-008 (**5**) and NPD-048 (**7**). The selectivity index (pK_i TbrPDEB1 – pK_i hPDE4) is indicated by colour.

the new TbrPDEB1 inhibitors, the SPR biosensor analysis indicates noteable differences in binding kinetics, as a much slower off-rates for TbrPDEB1 and hPDE4 can be observed when comparing the dissociation kinetics of **20** and **37**. The results indicate that binding kinetics represent an opportunity to design new compounds with improved activity profiles. We are currently developing *in silico* methods (including but not limited to molecular dynamics studies) to translate these kinetic binding data to molecular understanding.

2.6. Phenotypical data

All alkynamides were tested *in vitro* for their trypanocidal activity against *T. brucei* trypomastigotes (Table 3). The best results were obtained for **37** and **39**, which both displayed submicromolar activities and were not cytotoxic to MRC-5 cells. Aliphatic alkynamides (**20–27**) showed a lower activity when compared to alkynamides with aromatic tail groups (**11**, **12** and **28–41**), as observed in the biochemical assay.

As displayed in Fig. 7, the alkynamides showed a good correlation (R^2 = 0.7) between TbrPDEB1 and *T. brucei* activity. No correlation was observed between important physicochemical properties (cLogP, cLogS and TPSA) and their anti-*T. brucei* activity (graphic representation in Supporting Info). Most alkynamides showed low or no cytotoxicity on MRC-5 cells, except imidazole **36** that displayed a substantially higher cytotoxicity when compared with other alkynamides. When compared to alkynamide **7** (CC_{50} = 5.0) most decorated alkynamides show an improved cytotoxicity profile.

2.7. Intracellular real-time cAMP assay

To confirm on-target activity of **37** and **39** in live parasites, procyclic form trypanosomes expressing a FRET-based cAMP sensor were incubated with 1 and 10 μM inhibitor **37** and **39** (Fig. 8). Both inhibitors induce a rapid and sustained increase in intracellular cAMP in

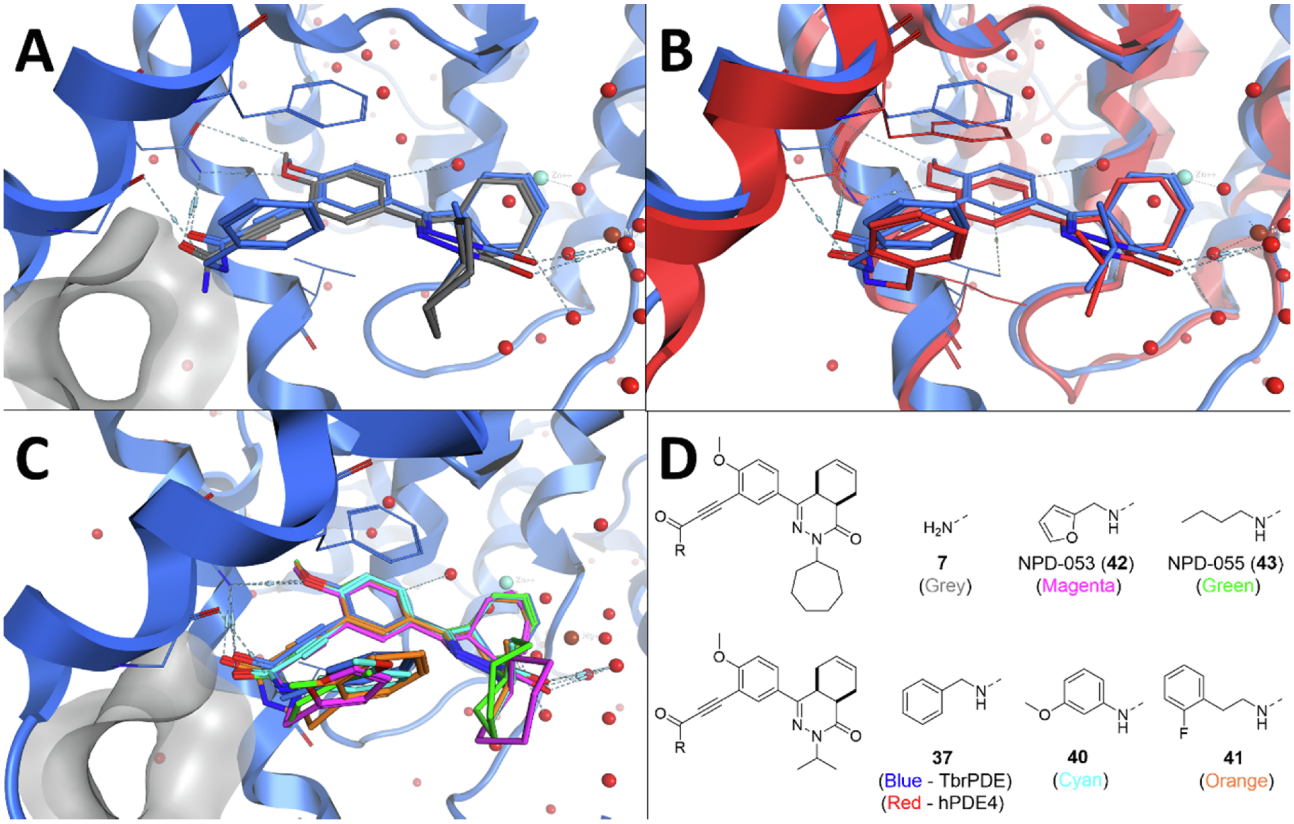

Fig. 5. Crystal structures of alkynamides in the catalytic domain of TbrPDEB1 (blue) and hPDE4 (red). Key residues, active site water molecules and metals are shown for clarity. A) Overlay of **7** (grey) and **37** (blue) in TbrPDEB1 with the P-pocket shown in grey. B) Binding pose of **37** in the catalytic domain of TbrPDEB1 (blue) and hPDE4 (red). C) Overlay of all obtained crystal structures of alkynamides **37** (blue), **40** (cyan) and **41** (orange), **42** (magenta) and **43** (green) bound to the catalytic domain of TbrPDEB1. D) Structures of the co-crystallized compounds and their colour of visualisation.

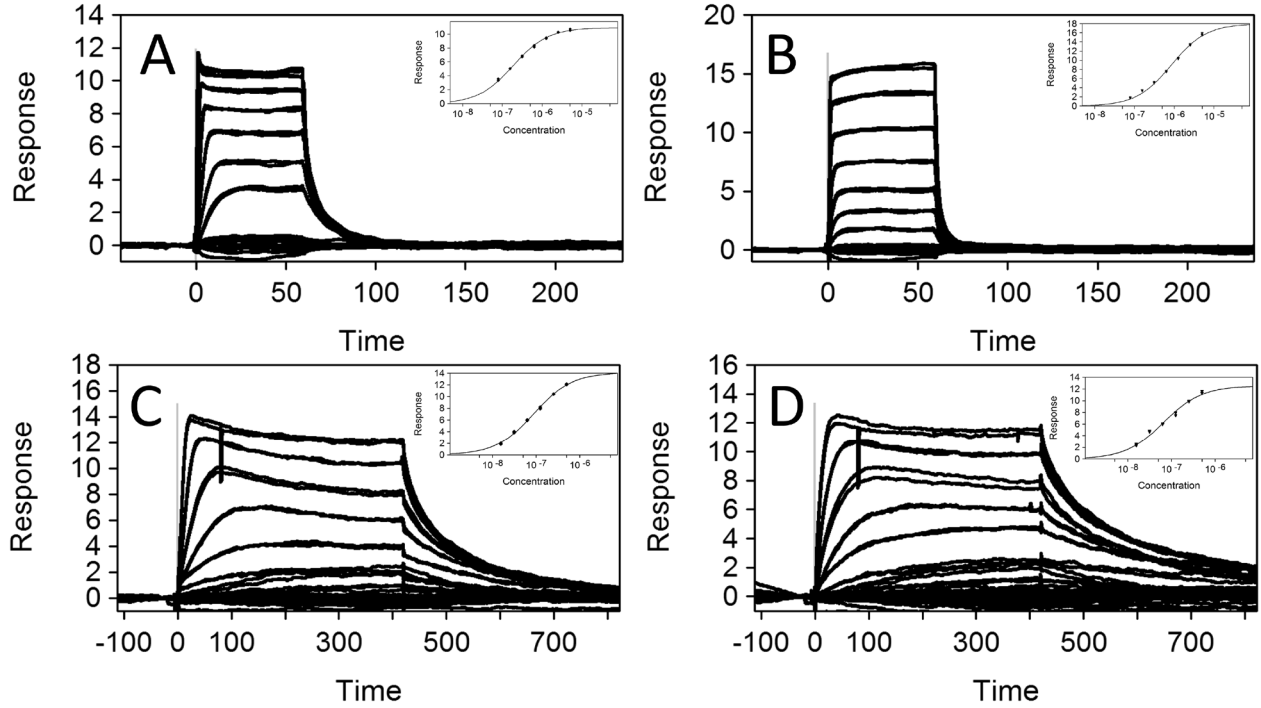

Fig. 6. Sensorgrams of compound **20** binding to hPDE4D (A) and TbrPDEB1 (B), and compound **37** binding to hPDE4D (C) and TbrPDEB1 (D). Inset shows steady-state affinity analyses of SPR biosensor interaction data; blank injections are also shown. Measurements using two independent biosensor chips and three different stock solutions indicate good reproducibility (see supplementary information).

Table 3
Trypanocidal activity of all alkynamides against *T. brucei* parasites and their cytotoxicity against human MRC-5 cells.

#	cLogP	cLogS	TPSA	*T. brucei* (pIC_{50})	MRC-5 (pCC_{50})
20	2.4	−4.3	85	5.2 ± 0.1	4.5 ± 0.1
21	3.9	−5.4	71	5.1 ± 0.1	< 4.2
22	3.4	−5.2	71	5.1 ± 0.1	< 4.2
23	3.8	−5.7	71	5.2 ± 0.1	< 4.2
24	2.4	−4.5	95	4.6 ± 0.1	4.5 ± 0.1
25	2.4	−4.9	86	5.1 ± 0.1	5.1 ± 0.1
26	3.0	−4.9	80	5.1 ± 0.1	4.5 ± 0.1
27	2.6	−4.7	71	5.0 ± 0.1	4.5 ± 0.1
11	3.0	−4.3	102	< 4.2	5.0 ± 0.2
12	3.7	−5.2	113	5.7 ± 0.1	5.1 ± 0.1
28	3.4	−5.3	84	5.6 ± 0.1	< 4.2
29	3.6	−5.5	84	5.5 ± 0.3	< 4.2
30	4.2	−5.9	71	6.0 ± 0.4	4.2 ± 0.1
31	4.5	−5.8	71	5.6 ± 0.1	< 4.2
32	3.2	−4.7	84	5.7 ± 0.1	4.9 ± 0.1
33	3.3	−4.6	84	5.3 ± 0.2	5.0 ± 0.1
34	3.4	−4.8	84	5.7 ± 0.1	5.1 ± 0.1
35	2.7	−4.0	89	5.8 ± 0.3	4.7 ± 0.1
36	2.6	−4.5	89	5.1 ± 0.1	6.6 ± 0.1
37	4.3	−5.9	71	6.2 ± 0.1	< 4.2
38	3.1	−4.7	84	5.9 ± 0.1	5.4 ± 0.2
39	3.1	−4.7	84	6.0 ± 0.4	4.5 ± 0.4
40	4.5	−6.0	80	5.8 ± 0.1	< 4.2
41	4.7	−6.1	71	5.7 ± 0.1	< 4.2

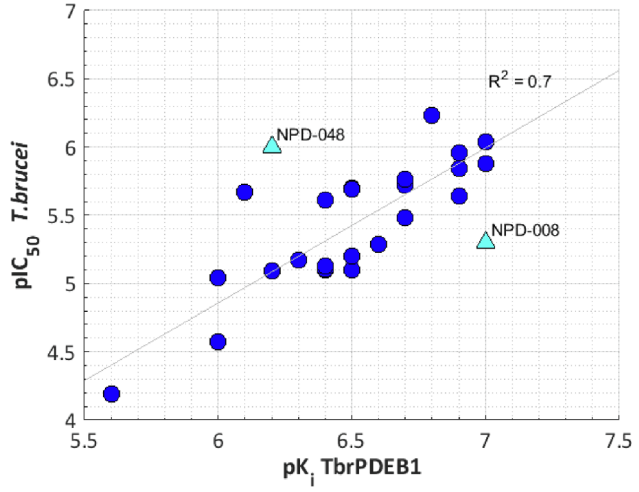

Fig. 7. Correlation between TbrPDEB1 activity and cellular activity against T. brucei parasites of all alkynamides and reference compounds NPD-048 and NPD-008.

the reporter cell line versus the negative control (DMSO), as indicated by an increase in 488/535 nm emission ratio. Both inhibitors were compared with a known non-selective TbrPDEB1 inhibitor (NPD-001), which was previously reported to increase intracellular cAMP levels in bloodstream and procyclic form trypanosomes.[18,33] Both inhibitors **37** and **39** show a higher response at 1 μM when compared with reference inhibitor NPD-001 and an equal response at 10 μM.

To determine the activity of inhibitor **37** and **39** on bloodstream form trypanosomes, parasites were incubated with inhibitor **37** and **39** for 24–48 h prior to fixation and cellular analysis by fluorescence microscopy. After incubation with inhibitor **37** and **39**, bloodstream form trypanosomes exhibit a lethal block in cytokinesis, indicated by multi-nucleated and multi-flagellated parasites (Fig. 9). The trypanocidal effects of **37** and **39** are in line with previous observations after genetic and pharmacological modulation of TbrPDEB1 and TbrPDEB2 expression or function in bloodstream form trypanosomes.[16,19]

3. Conclusion

The structure-based design of alkynamide phthalazinones as TbrPDEB1 inhibitors delivered several compounds with a sub-micromolar activity against TbrPDEB1 and a modest selectivity over its human homologue hPDE4. Unexpectedly, alkynamide **37** did not show the predicted P-pocket occupation by the tail group in the co-crystal structure with TbrPDEB1 and a very similar binding mode was observed in the co-crystal structure with hPDE4. This observation indicates that targeting of the P-pocket of TbrPDEB1 is difficult to achieve with alkynamide tetrahydrophthalazinones. Moreover, the observed (moderate) selectivity of the benzyl and the two pyridinyl-substituted alkynamides **37**, **38** and **39** suggests that other, as of yet unidentified interactions of PDE inhibitors with TbrPDEB1 and hPDE4 can also result in (moderate) parasite selectivity. The alkynamides show a good correlation between their biochemical activity against TbrPDEB1 and their *in vitro* activity against *T. brucei* parasites. Benzyl alkynamide **37** (NPD-1335) is 5-fold more potent against TbrPDEB1 (pK_i = 6.9) than hPDE4 (pK_i = 6.2) and displays a greatly improved cytotoxicity profile (pIC_{50} *T. brucei* = 6.2 *vs* pCC_{50} MRC-5 < 4.2) when compared to the unsubstituted alkynamide **7** (pIC_{50} *T. brucei* = 6.0 *vs* pCC_{50} MRC-5 < 5.0). Furthermore, incubation of procyclic forms with **37** and **39** results in elevation of the intracellular cAMP levels in the cells. In bloodstream forms, incubation with **37** and **39** leads to a block in cytokinesis, which is associated with formation of multiple flagella and nuclei, both supporting a PDE-mediated mode of action.

4. Experimental

4.1. Docking

The dockings were performed similar to the combined screening protocol as previously published for GPCRs.[30] In short, the dockings were performed using PLANTS[28] (version 1.2) and the resulting docking poses were post-processed with IFP[29] (version 2.2). Every molecule was docked 5 times generating 10 docking poses during each iteration (speed setting 2, RMSD 1.0) into each of the three crystal structures (chain B for 5G2B and 5L8Y and chain A for 6FTM) based on the pocket definition as defined for PDEStrIAn.[34] All docking poses were scored using the ChemPLP scoring function and only poses with a score ≤ −90 were further investigated. The positioning of the core scaffold was evaluated by performing an IFP similarity comparison to the co-crystallized ligands limited to solely the residues in the direct vicinity of the core scaffold. Poses with an IFP score lower than 0.5 or where the ligand did not interact with the conserved glutamine (Q.50) or the hydrophobic clamp (HC.32, HC.52) were removed. A final interaction filter was applied to select only those binding modes in which the Q2 pocket was targeted by having at least one IFP contact with Q2.45 or Q2.46. From the initial combinatorial library of 16,153 alkynamides 2291 compounds remained for further processing.

4.2. Protein production

Cloning, expression and purification of recombinant TbrPDEB1 and hPDE4D catalytic domains were performed as previously described.[25]

4.3. Crystallization, data collection and structure determination

Apo crystals of TbrPDEB1 and hPDE4D were grown in 24 well XRL plates (Molecular Dimensions, Newmarket, Suffolk, UK) by vapor diffusion hanging drop technique. Typically, protein and crystallization solution were mixed in 1:1 ratio and drops were setup against 500 μL reservoir solution. Crystals of TbrPDEB1 were obtained in a condition containing 20% PEG 3350, 400 mM sodium formate, 300 mM guanidine and 100 mM MES pH 6.5 at 4 °C and soaked with different inhibitors to obtain protein-inhibitor complexes. hPDE4D crystals

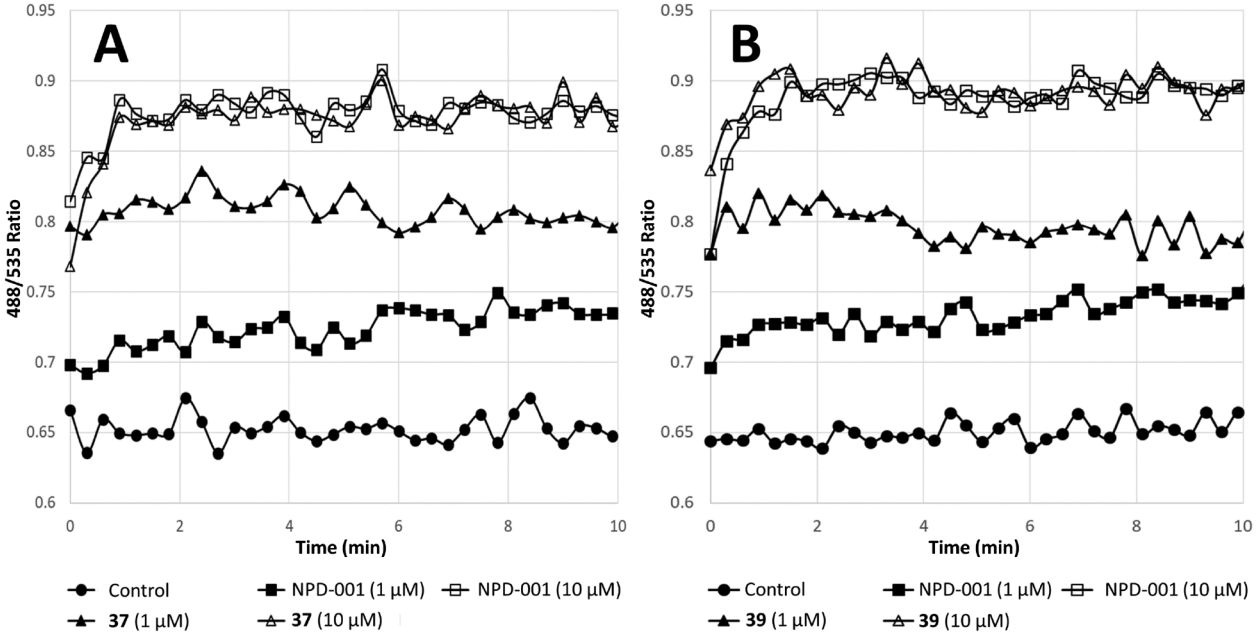

Fig. 8. Intracellular cAMP levels in procyclic form trypanosomes upon incubation with inhibitor A) **37** and B) **39** at two concentrations (1 μM and 10 μM) compared to NPD-001 and control cells.

obtained in a condition containing 24% PEG 3350, 30% ethylene glycol and 100 mM HEPES pH 7.5 at 19 °C were complexed with different inhibitors in a similar way. The soaked crystals were then cryo protected, mounted on CryoLoop (Hampton Research, Aliso Viejo, CA, USA) or LithoLoops (Molecular Dimensions) and vitrified in liquid nitrogen for data collection. All X-ray diffraction data sets were collected

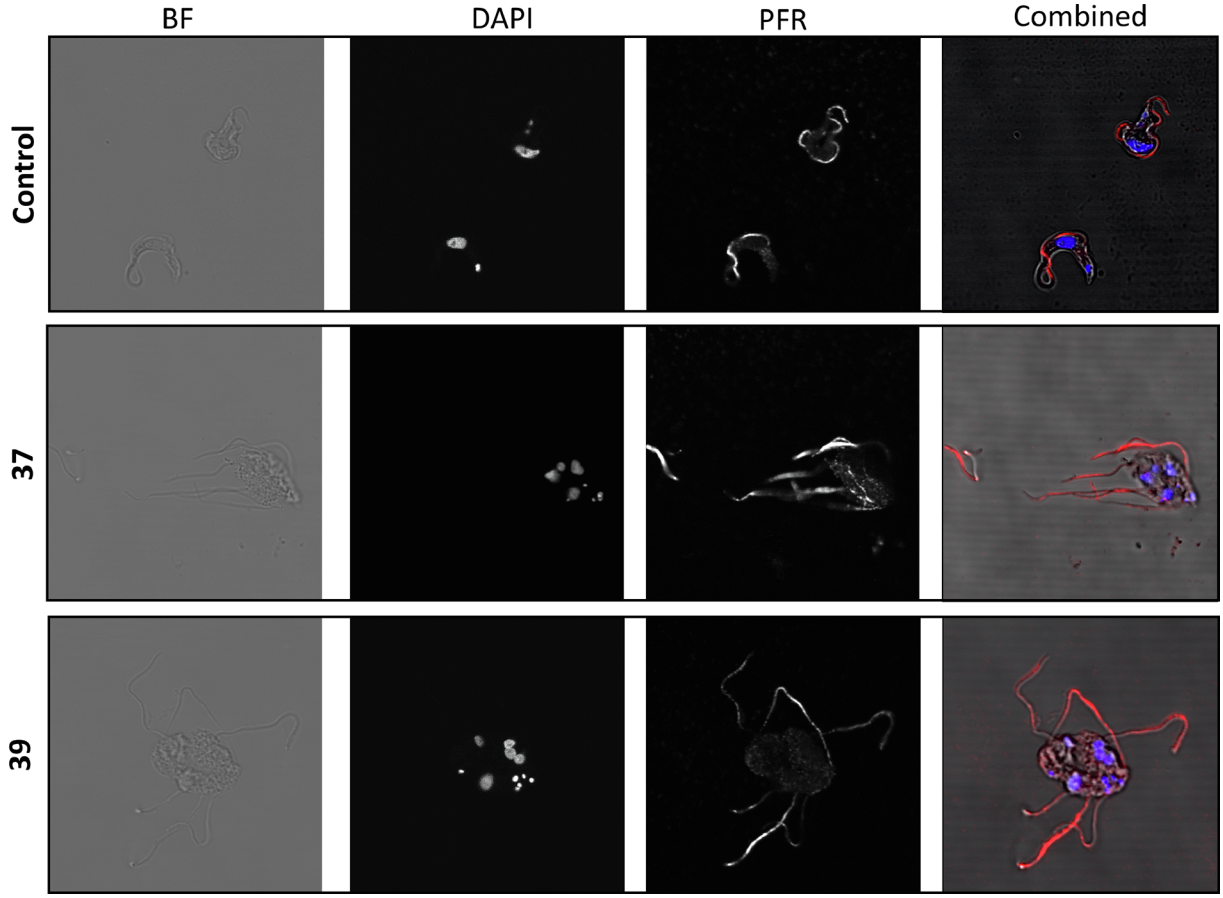

Fig. 9. Fluorescence microscopy of control trypanosomes and trypanosomes incubated with **37** or **39** after 24–48 h visualized with different stains. First column shows cells under normal microscope conditions. Second and third column show the cells with DAPI and PFR stains respectively to visualise cell nuclei (DAPI) and the flagellum (PFR). Overlay of the different imaging techniques is shown in the fourth column.

Table 4
Data collection and refinement statistics for TbrPDEB1 crystals bound to various inhibitors.

Data collection	NPD-1335	NPD-1018	NPD-1039	NPD-053	NPD-055
Synchrotron and Beamline	Diamond I04-1	Diamond I03	Diamond I03	Diamond I04-1	Diamond I03
Space group	C2	C2	C2	C2	C2
Molecule/a.s.u	2	2	2	2	2
Celll dimensions *a*, *b*, *c* (Å)	114.73, 114.54, 68.20	114.71, 116.08, 68.67	113.72, 116.55, 68.53	147.51, 115.07, 63.78	114.78, 116.48, 68.61
α,β,γ (°)	90, 108.28, 90	90, 108.26, 90	90, 108.17, 90	90, 109.39, 90	90, 108.32, 90
Resolution (Å)	64.76–1.96 (2.01–1.96)*	65.21–2.28 (2.29–2.28)	65.11–2.18 (2.19–2.18)	69.57–1.90 (1.94–1.90)	79.57–2.03 (2.08–2.03)
R_{merge}	0.09 (0.70)	0.07 (0.55)	0.04 (0.57)	0.09 (0.62)	0.06 (1.17)
I/σ*I*	6.0 (1.3)	10.7 (2.3)	15.3 (2.1)	7.2 (2.0)	11.5 (1.1)
CC(1/2)	0.99 (0.59)	0.99 (0.86)	0.99 (0.88)	0.99 (0.47)	0.99 (0.59)
Completeness (%)	99.8 (99.9)	98.3 (96.5)	96.9 (97.7)	99.7 (99.9)	99.7 (99.7)
Redundancy	3.3 (3.3)	3.4 (3.3)	3.3 (3.3)	3.1 (3.3)	3.4 (3.4)
Refinement					
Resolution (Å)	1.96	2.29	2.18	1.90	2.03
No. reflections	55,439	36,118	40,644	74,823	52,428
R_{work}/R_{free}	0.20/0.24	0.16/0.22	0.17/0.23	0.16/0.19	0.18/0.23
No. atoms					
Protein	5260	5260	5248	5278	5260
Water	433	339	270	418	336
B-factors (Å^2)					
Protein	41.07	50.51	58.70	31.72	51.64
Water	45.80	48.19	53.60	41.87	52.77
Ligand	54.00	80.61	76.37	47.54	62.12
R.m.s. deviations					
Bond lengths (Å)	0.008	0.010	0.009	0.010	0.007
Bond angles (°)	1.247	1.683	1.558	1.713	1.465
PDB accession code	6GXQ	6RFN	6RFW	6RB6	6RGK
PDB ligand code	FFZ	K3W	K1Q	JX2	K3N

Data collected from a single crystal.
*Values in parentheses are for highest-resolution shell

Table 5
Data collection and refinement statistics for hPDE4D crystals bound to NPD-1335 and NPD-053.

Data collection	NPD-1335	NPD-053
Synchrotron and Beamline	Diamond I04-1	Diamond I03
Space group	$P2_12_12_1$	$P2_12_12_1$
Molecule/a.s.u	4	4
Cell dimensions *a*, *b*, *c* (Å)	98.54, 110.89, 160.39	99.89, 110.50, 160.69
α,β,γ (°)	90, 90, 90	90, 90, 90
Resolution (Å)	80.19–1.99 (2.04–1.99)*	160.69–2.07 (2.08–2.07)
R_{merge}	0.06 (0.70)	0.06 (0.79)
I/σ*I*	14.1 (2.0)	16.2 (2.0)
CC(1/2)	0.99 (0.58)	0.99 (0.75)
Completeness (%)	100 (1 0 0)	99.9 (94.8)
Redundancy	6.5 (6.6)	6.6 (6.8)
Refinement		
Resolution (Å)	1.99	2.08
No. reflections	112,544	102,189
R_{work}/R_{free}	0.20/0.25	0.17/0.22
No. atoms		
Protein	10,501	10,524
Water	590	658
B-factors (Å^2)		
Protein	43.39	47.59
Water	44.00	52.99
Ligand	64.02	88.92
R.m.s. deviations		
Bond lengths (Å)	0.019	0.01
Bond angles (°)	1.935	1.653
PDB accession code	6HWO	6RCW
PDB ligand code	FFZ	JX2

*Values in parentheses are for highest-resolution shell.

at Diamond Light Source (DLS; Didcot, Oxfordshire, UK) at beam lines I03 using a Pilatus 6 M detector (Dectris, Baden, Switzerland) or at I04-1 using a Pilatus 6 M − F detector (Dectris) at 100 K temperature. Datasets were processed with xia2[35] or autoPROC[36] pipelines available at DLS, which incorporates XDS[37] and AIMLESS,[38] or were integrated using iMOSFLM[39] and reduced using POINTLESS, AIMLESS and TRUNCATE, all of which are part of CCP4 suite.[40] Structures of inhibitor complexes with TbrPDEB1 and hPDE4D were determined by molecular replacement in CCP4 suite program PHASER[41] by using the respective apo models (TbrPDEB1, PDB id: 4I15; hPDE4D, PDB id: 3SL3) as search templates. Stereochemical restrains for the inhibitors were generated by ACEDRG available within the CCP4 package and ligand fitting and model adjustment were carried out in COOT[42] followed by their refinement in REFMAC.[43] Data processing and refinement statistics are given in Tables 4 and 5. Structural figures were prepared with PYMOL[44]. Coordinates of the structures have been deposited to the RCSB Protein Data Bank with following accession codes: 6GXQ (TbrPDEB1-NPD-1335), 6RFN (TbrPDEB1-NPD-1018), 6RFW (TbrPDEB1-NPD-1039), 6RB6 (TbrPDEB1-NPD-053), 6RGK (TbrPDEB1-NPD-055), 6HWO (hPDE4D-NPD-1335) and 6RCW (hPDE4D-NPD-053).

4.4. Phosphodiesterase activity assays

Phosphodiesterase activity assays are performed using the PDELight™ HTS cAMP phosphodiesterase Kit (Lonza, Walkersville, USA): The assay is performed at 25 °C in non-binding, low volume 384 wells plates (Corning, Kennebunk, ME, USA). PDE activity measurements (TbrPDEB1_CD; K_m 3.45 μM, hPDE4B_CD; K_m 13.89 μM) are made in 'stimulation buffer' (50 mM Hepes, 100 mM NaCl, 10 mM MgCl, 0.5 mM EDTA, 0.05 mg/mL BSA, pH 7.5). Single concentration measurements are made at 10 μM inhibitor concentration (triplo

measurements/assay, n = 2). Dose response curves are made in the range 100 μM − 10 pM (triplo measurements/assay, n = 3). Compounds are diluted in DMSO (final concentration 1%). Inhibitor dilutions (2.5 μL) are transferred to the 384 wells plate, 2.5 μL PDE in stimulation buffer is added and mixed, 5 μL cAMP (at 2 × K_m up to 20 μM) is added and the assay is incubated for 20 min at 300 rpm. The reaction is terminated by then addition of 5 μL Lonza Stop Buffer supplemented with 10 μM NPD-001. Then 5 μL of Lonza Detection reagent (diluted to 80% with reaction buffer) is added and the reaction incubated for 10 min at 300 rpm. Luminescence is read with a Victor3 luminometer using a 0.1 s/well program.

RLUs were measured in comparison to the DMSO-only control, NPD-001 always was taken along as positive control as a PDE inhibitor. The K_i values of the inhibitors analyzed are represented as the mean of at least three independent experiments with the associated standard error of the mean (SEM) as indicated.

4.5. Phenotypic cellular assays

For the cellular assays, the following reference drugs were used as positive controls: suramin (Sigma-Aldrich, Germany) for T. brucei (pIC_{50} = 7.4 ± 0.2, n = 5), and tamoxifen (Sigma-Aldrich, Germany) for MRC-5 cells (pCC_{50} = 5.0 ± 0.1, n = 5). All compounds were tested at five concentrations (64, 16, 4, 1 and 0.25 μM) to establish determination of the IC_{50} and CC_{50}. Data are represented as the mean of duplicate experiments ± S.E.M. The final concentration of DMSO did not exceed 0.5% in the assays.

In vitro antitrypanosomal assay. *T. brucei* Squib-427 strain (suramin-sensitive) was cultured at 37 °C and 5% CO_2 in HMI-9 medium, supplemented with 10% heat-inactivated fetal calf serum (FCSi). About 1.5 × 10^4 trypomastigotes were added to each well and parasite growth was assessed after 72 h at 37 °C by adding resazurin. Viability was assessed fluorimetrically 24 h after the addition of resazurin. Fluorescence was measured (excitation 550 nm, emission 590 nm) and the results were expressed as percentage reduction in viability compared to control.

In vitro MRC-5 cytotoxicity assay. MRC-5 SV2 cells, originally from a human diploid lung cell line, were cultivated in MEM, supplemented with L-glutamine (20 mM), 16.5 mM sodium hydrogen carbonate and 5% FCSi. For the assay, 10^4 MRC-5 cells/well were seeded onto the 96-well test plates containing the pre-diluted sample and incubated at 37 °C and 5% CO_2 for 72 h. Cell viability was assessed fluorimetrically 4 h after the of addition of resazurin. Fluorescence was measured (excitation 550 nm, emission 590 nm) and the results were expressed as percentage reduction in cell viability compared to control.

4.6. Intracellular cAMP and fluorescence microscopy

4.6.1. Cell lines

Procyclic 2913 *T. b. brucei*[45] were cultivated in SDM-79 supplemented with 5% FCSi[46] Bloodstream-form *T. b. brucei* 221 single marker cell line[45] were cultivated in HMI-9 medium supplemented with 10% FCSi[46] The cAMP FRET reporter cell line was developed by transfecting 2913 procyclic form *T. b. brucei* with linearized pLEW-100 containing epac1camps. Selection for transfected cells and cloning by limited dilution was done as published previously.[46] Expression of epac1-camps was validated using fluorescence microscopy.

4.6.2. Plasmids

For tetracycline inducible expression of the cAMP FRET sensor, the Epac1camps sensor[47] was cloned into pLEW-100[45] as described.[33]

4.6.3. Chemicals

NPD-001, **37**, **39** were dissolved in DMSO to 1 and 10 mM and stored at −80 °C.

4.6.4. FRET assay

cAMP FRET assays were performed in triplicates for each time point and 3 independent experiments, as described previously[33]: As controls, NPD-001 (positive control,[18] and DMSO (solvent for **37**, **39**, NPD-001)) were included. The following modifications to the published method[33] were made: the cAMP reporter cell line was cultivated in SDM-79 containing 5% FCSi. After induction of Epac1-camps expression with tetracycline[46] for 24 h-48 h, the cells were washed once and re-suspended in PBS containing 5% FCSi to 1.5 × 10^8 cells/mL. 150 μL of cells was added to each well of a 96-well black microtiter plate. 50 μL of NPD-001, **37**, **39** and DMSO diluted in PBS containing 5% FCSi was added to the wells (final concentration of compounds: 10 μM).

4.6.5. Microscopy

Bloodstream-form *T. b. brucei* 221 single marker cell line were cultivated for 24 h in the presence of 1 μM NPD-001, **37**, **39** or DMSO as control. Methodology used for cell fixation and staining has been described previously,[48] with the following modifications: blocking and antibody staining was done in PBS containing 5% bovine serum albumin (BSA). Antibodies used were rat anti-PFR 1:500[49] and anti-rat Alexa594 1:500 (Invitrogen). NucBlue Fixed Cell Stain (Invitrogen) was added to Vectashield mounting medium (for DNA stain). Images were acquired using a Leica confocal microscope and standard procedures. Images were processed using ImageJ.

4.7. Surface plasmon resonance

All experiments were performed with a Biacore T200 surface plasmon resonance biosensor instrument (GE healthcare). Proteins were immobilized on CM5 series S sensor chips. Consumables were obtained from GE Healthcare. All solutions were freshly prepared, degassed, and filtered. The neutravidin immobilization was run on HBS-N at a flowspeed of 10 μL/min at 25 °C. The matrix of the sensor chip was activated by injecting on all flow channels a mixture of 0.1 M *N*-hydroxysuccinimide (NHS) and 0.4 M 1-ethyl-3-(3-(dimethylamino) propyl) carbodiimidehydrochloride (EDC) at a flow rate of 10 μM for 420 s. Subsequently, neutravidin (0.30 mg/mL) in a 10 mM NaAc solution (pH 5.0) was injected for 120 s. Unreacted activated groups of the dextran matrix were deactivated by injection of ethanolamine.HCl (1 M) for 420 s.

The catalytic domains of hPDE4D and TbrPDEB1 were produced and purified as previously described.[25] the proteins were buffer exchanged using a Amicon Ultra 0.5 mL centrifugal filter (Merk) to HBS-N, 5% glycerol (v/v), 4 μM $MgCl_2{\cdot}6H_2O$, 100 nM $ZnCl_2$, 2 mM 2-mercaptoethanol and diluted to 1 mg/mL. EZ-Link Sulfo-NHS-Biotin (Thermo Fisher Scientific) was diluted to 1.5 mM in the same buffer, mixed with the protein in a 1:1 M ratio, and incubated at 4 °C overnight. Biotinylated proteins were buffer exchanged to 0.5 M Tris-HCl (pH 8.0), 150 mM NaCl, 4 mM $MgCl_2{\cdot}6H_2O$, 100 nM $ZnCl_2$, 5% glycerol (v/v), 2 mM 2-mercaptoethanol, and desalted using 0.5 mL Zeba Spin desalting columns (Thermo Scientific). Proteins were diluted to 0.5 mg/mL and injected on the flow channels until 3000 RU in the same buffer at 15 °C. Biocytin (0.05 mg/mL) was injected for 120 s on all flow channels at 15 °C.

All compounds were dissolved in DMSO (stock solutions of 10 mM) and diluted in 0.5 M Tris-HCl (pH 8.0), 150 mM NaCl, 4 mM $MgCl_2{\cdot}6H_2O$, 100 nM $ZnCl_2$, 5% glycerol (v/v), 2 mM 2-Mercaptoethanol, 0.005% Tween-20 (v/v), 2% DMSO (v/v). Suitable concentration series and injection times were determined for each compound separately. In multicycle experiments, a 7-point concentration range of each compound was measured. On a first CM5 chip, a first stock solution was used to obtain a dose response curve in duplicate. On a second CM5 chip, two other independent stock solutions were used to measure dose response curves in duplicate. Compound **20** was injected for 60 s and its dissociation was monitored for 300 s. Compound **37** was injected for 420 s and its dissociation was monitored for 900 s. All

titrations were run at 25 °C at a flow speed of 50 μL/min. Data analyses were performed with Scrubber2. Signals were subtracted from reference surface and blanc injections. DMSO correction was performed. The affinity was determined by fitting a Langmuir binding equation to steady state binding signals at different concentrations. All SPR experiments are shown in the Supplementary data with individually measured pK_D and the error reported is the error in the fit of the binding isotherm.

4.8. Chemistry

4.8.1. General

All reagents and solvents were obtained from commercial suppliers and were used as received. All reactions were magnetically stirred and carried out under an inert atmosphere. Reaction progress was monitored using thin-layer chromatography (TLC) and LC-MS analysis. LC-MS analysis was performed on a Shimadzu LC-20AD liquid chromatograph pump system, equipped with an Xbridge (C18) 5 μm column (50 mm, 4.6 mm), connected to a Shimadzu SPD-M20A diode array detector, and MS detection using a Shimadzu LC-MS-2010EV mass spectrometer. The LC-MS conditions were as follows: solvent A (water with 0.1% formic acid) and solvent B (acetonitrile with 0.1% formic acid), flow rate of 1.0 mL/min, start 5% B, linear gradient to 90% B in 4.5 min, then 1.5 min at 90% B, then linear gradient to 5% B in 0.5 min, then 1.5 min at 5% B; total run time of 8 min. Silica gel column chromatography was carried out with automatic purification systems using the indicated eluent. Reversed phase column purification was performed on Grace Davison iES system with C18 cardridges (60 Å, 40 μm) using the indicated eluent. Nuclear magnetic resonance (NMR) spectra were recorded as indicated on a Bruker Avance 500 (500 MHz for ^{1}H and 125.8 MHz for ^{13}C) instrument equipped with a Bruker CryoPlatform, or on a Bruker Avance III HD (600 MHz for ^{1}H) instrument equipped with a Bruker CryoPlatform. Chemical shifts (δ in ppm) and coupling constants (*J* in Hz) are reported with residual solvent as internal standard (δ ^{1}H NMR: $CDCl_3$ 7.26; DMSO-d_6 2.50; δ ^{13}C NMR: $CDCl_3$ 77.16; DMSO-d_6 39.52). Abbreviations used for ^{1}H NMR descriptions are as follows: s = singlet, d = doublet, t = triplet, q = quintet, hept = heptet dd = doublet of doublets, dt = doublet of triplets, tt = triplet of triplets, m = multiplet, app d = apparent doublet, br = broad signal. Exact mass measurement (HRMS) was performed on a Bruker micrOTOF-Q instrument with electrospray ionization (ESI) in positive ion mode and a capillary potential of 4,500 V. Systematic names for molecules were generated with ChemBioDraw Ultra 14.0.0.117 (PerkinElmer, Inc.). The reported yields refer to isolated pure products and yields were not optimized. The purity, reported as the LC peak area % at 254 nm, of all final compounds was ≥95% based on LC-MS. All compounds are isolated as a racemic mixture of *cis*-enantiomers.

4.8.2. Synthetic procedures

*4.8.2.1. (E)-4-(3-Bromo-4-methoxyphenyl)-4-oxobut-2-enoic acid (**14**).* To an ice-cooled mixture of 1-bromo-2-methoxybenzene (65 mL, 0.52 mol) and furan-2,5-dione (77 g, 0.78 mol) in DCM (465 mL) was added $AlCl_3$ (84 g, 0.63 mol). The reaction mixture was stirred at rt overnight. The orange suspension was quenched in 3 M aq. HCl (1.5 L) and extracted using EtOAc (4 × 1 L). The combined organic layers were dried over Na_2SO_4, filtered and concentrated to obtain a dark yellow solid. Trituration with Et_2O provided the product as a light yellow solid (97.5 g, 66%).

LC-MS (ESI): t_R = 4.09 min, area: > 98%, *m/z*: 285/287 $[M+H]^+$.

^{1}H NMR (500 MHz, $CDCl_3$): δ 7.89 (d, *J* = 2.2 Hz, 1H), 7.69 (dd, *J* = 8.7, 2.2 Hz, 1H), 7.53 (d, *J* = 15.4 Hz, 1H), 6.74 (d, *J* = 8.7 Hz, 1H), 6.51 (d, *J* = 15.4 Hz, 1H), 3.69 (s, 3H).

^{13}C NMR (126 MHz, DMSO-d_6): δ 187.2, 167.1, 166.7, 160.2, 136.3, 133.8, 133.0, 131.3, 130.6, 112.9, 111.8, 57.3.

HRMS (ESI): *m/z*: $[M+H]^+$ calcd. for $C_{11}H_{10}BrO_4$ 284.9757, found 284.9763.

*4.8.2.2. Trans-6-(3-Bromo-4-methoxybenzoyl)cyclohex-3-ene-1-carboxylic acid (**15**).* A mixture of **14** (70.0 g, 221 mmol) and buta-1,3-diene in THF (~13% w/w, 150 mL, 300 mmol) was divided over 8 microwave vials. Each vial was stirred under microwave irradiation at 140 °C for 30 min (the internal pressure reached ~ 10 bar). The reaction mixtures were pooled and concentrated *in vacuo* to obtain the crude product. Trituration with toluene provided the product as a white solid (72.4 g, 97%).

LC-MS (ESI): t_R = 4.53 min, area: > 98%, *m/z*: 339/341 $[M+H]^+$

^{1}H NMR (500 MHz, DMSO-d_6): δ 12.30 (s, 1H), 8.16 (s, 1H), 8.07 (d, *J* = 8.7 Hz, 1H), 7.23 (d, *J* = 8.5 Hz, 1H), 5.79–5.66 (m, 2H), 3.95 (s, 3H), 3.83–3.72 (m, 1H), 2.92–2.75 (m, 1H), 2.54–2.10 (m, 3H), 1.93–1.79 (m, 1H).

^{13}C NMR (126 MHz, DMSO-$_6$): δ 200.8, 176.4, 159.61 133.4, 130.6, 130.3, 125.8, 125.7, 112.8, 111.6, 57.2, 42.2, 41.6, 29.4, 28.4.

HRMS (ESI): *m/z*: $[M+H]^+$ calcd. for $C_{15}H_{16}BrO_4$ 339.0226, found 339.0213

*4.8.2.3. Trans-4-(3-Bromo-4-methoxyphenyl)-4a,5,8,8a-tetrahydrophthalazin-1(2H)-one (**16**).* A solution of **15** (70 g, 0.21 mol) and hydrazine monohydrate (32 mL, 0.62 mol) in EtOH (400 mL) was stirred at reflux for 4 h. The reaction mixture was cooled in the refridgerator and filtered to obtain the pure product as a white solid (60 g, 86%). Note: Partial conversion of stereochemistry during the condensation reaction was observed only once (out of 5) during a small scale reaction (< 3 mmol).

LC-MS (ESI): t_R = 4.29 min, area: > 98%, *m/z*: 335/337 $[M+H]^+$.

^{1}H NMR (600 MHz, DMF-d_7) δ 10.98 (s, 1H), 7.74 (d, *J* = 2.1 Hz, 1H), 7.52 (dd, *J* = 8.5, 2.1 Hz, 1H), 7.22 (d, *J* = 8.5 Hz, 1H), 5.82–5.64 (m, 2H), 3.98 (s, 3H), 3.14 (ddd, *J* = 14.6, 11.4, 5.4 Hz, 1H), 2.57 (td, *J* = 14.2, 13.3, 5.4 Hz, 2H), 2.51–2.43 (m, 1H), 2.22–2.10 (m, 1H), 1.94–1.84 (m, 1H).

^{13}C NMR (126 MHz, DMSO-d_6): δ 168.9, 155.9, 153.8, 132.3, 130.9, 128.7, 126.1, 125.9, 112.4, 110.5, 56.8, 36.2, 34.3, 30.3, 26.2.

HRMS (ESI): *m/z*: $[M+H]^+$ calcd. for $C_{15}H_{16}BrN_2O_2$ 335.0390, found 335.0378.

*4.8.2.4. Cis-4-(3-Bromo-4-methoxyphenyl)-2-isopropyl-4a,5,8,8a-tetrahydrophthalazin-1(2H)-one (**17**).* To a solution of **16** (50.0 g, 0.15 mol) in DMF (500 mL) was added NaH (15 g, 0.37 mol) and the reaction mixture was stirred at rt for 30 min. 2-bromopropane (21 mL, 22 mmol) was added to the reaction mixture and the reaction mixture was stirred at rt for 4 h. The reaction mixture was quenched with aq. HCl (0.5 M, 1.5 L) on ice. The suspension was filtered and the residue was dissolved in MeOH/DCM. The solution was dried over Na_2SO_4, filtered and concentrated *in vacuo*. The residue was triturated with Et_2O to obtain the product as white crystals (46 g, 81%).

LC-MS (ESI): t_R = 5.30 min, area: > 98%, *m/z*: 377/379 $[M+H]^+$.

^{1}H NMR (600 MHz, $CDCl_3$) δ 8.04 (s, 1H), 7.74 (d, *J* = 8.6 Hz, 1H), 6.94 (d, *J* = 8.6 Hz, 1H), 5.85–5.65 (m, 2H), 5.05 (hept, *J* = 6.3 Hz, 1H), 3.95 (s, 3H), 3.28 (dt, *J* = 11.5, 5.8 Hz, 1H), 3.07–2.96 (m, 1H), 2.74 (t, *J* = 6.1 Hz, 1H), 2.26–2.12 (m, 2H), 2.08–1.96 (m, 1H), 1.33 (d, *J* = 6.6 Hz, 3H), 1.22 (d, *J* = 6.7 Hz, 3H).

^{13}C NMR (126 MHz, DMSO-d_6): δ 166.5, 156.8, 152.9, 130.4, 129.2, 127.3, 126.3, 124.4, 113.0, 111.6, 56.9, 46.2, 34.3, 30.3, 22.9, 22.4, 20.9, 20.6.

HRMS (ESI): *m/z*: $[M+H]^+$ calcd. for $C_{18}H_{22}BrN_2O_2$ 377.0859, found 377.0871.

*4.8.2.5. Trimethyl(3,3,3-triethoxyprop-1-yn-1-yl)silane (**18**).* Magnesium (1.38 g, 56.7 mmol) was activated using a mortar and pestle and was suspended in dry Et_2O (25 mL). 2-bromopropane (5.33 mL, 56.7 mmol) was slowly added to the stirring reaction mixture while cooling with water (the reaction mixture starts to reflux). The reaction mixture was stirred in a cold water bath for 30 min prior to the addition of ethynyltrimethylsilane (6.68 mL,

47.3 mmol). This reaction mixture was stirred for an additional 30 min to form a thick grey suspension, which was diluted with Et_2O (25 mL) prior to slow addition of tetraethoxymethane (10.9 mL, 52.0 mmol). After 1 h the reaction mixture turned into a dark brown/colourless mixture (two phases). The reaction mixture was poured in saturated aq. NH_4Cl (500 mL) and was extracted with Et_2O (2 × 500 mL). The organic phase was concentrated and the product was isolated as a light yellow liquid (10.5 g, 93%).

^{1}H NMR (500 MHz, DMSO-d_6): δ 3.55 (q, J = 7.1 Hz, 6H), 1.12 (t, J = 7.2 Hz, 9H), 0.18 (s, 9H).

^{13}C NMR (126 MHz, DMSO-d_6): δ 107.8, 99.2, 88.0, 58.3, 14.7, −0.5.

HRMS (ESI): m/z: $[M+Na]^+$ calcd. for $C_{12}H_{24}NaO_3Si$ 267.1387, found 267.1376.

*4.8.2.6. Ethyl 3-(5-(cis-3-isopropyl-4-oxo-3,4,4a,5,8,8a-hexahydrophthalazin-1-yl)-2-methoxyphenyl)propiolate (**19**).* To a N_2-purged solution of **17** (0.50 g, 1.3 mmol) in DMF (2 mL) and Et_3N (2 mL) was added subsequently **18** (0.65 g, 2.7 mmol), $PdCl_2$(dppf) (49 mg, 0.66 mmol), CuI (25 mg, 0.13 mmol) and CsF (0.30 g, 1.99 mmol). The mixture was stirred in the microwave at 120 °C for 4 h. The reaction mixture was poured in 1 M aq. HCl (250 mL) and extracted with EtOAc (2 × 250 mL). The organic phase was washed with brine (250 mL), dried over $MgSO_4$, filtered and concentrated to obtain the crude product as a brown solid. The crude product was purified using flash column chromatography (0–50% EtOAc/Hept). The product was obtained as a light yellow solid (0.37 g, 70%).

LC-MS (ESI): t_R = 5.31 min, area: > 98%, m/z: 395 $[M+H]^+$.

^{1}H NMR (500 MHz, DMSO-d_6): δ 8.10–7.99 (m, 2H), 7.25 (d, J = 8.9 Hz, 1H), 5.74–5.56 (m, 2H), 4.88 (hept, J = 6.6 Hz, 1H), 4.25 (q, J = 7.1 Hz, 2H), 3.93 (s, 3H), 3.51 (dt, J = 11.5, 5.8 Hz, 1H), 2.80 (t, J = 6.0 Hz, 1H), 2.78–2.69 (m, 1H), 2.23–2.06 (m, 2H), 1.86–1.72 (m, 1H), 1.33–1.20 (m, 6H), 1.15 (d, J = 6.8 Hz, 3H).

^{13}C NMR (126 MHz, DMSO-d_6): δ 166.6, 162.5, 153.6, 153.0, 132.3, 131.1, 128.1, 126.3, 124.5, 112.6, 108.1, 84.9, 82.9, 62.5, 56.8, 46.2, 34.3, 30.2, 22.8, 22.4, 20.9, 20.6, 14.4.

HRMS (ESI): m/z: $[M+H]^+$ calcd. for $C_{23}H_{27}N_2O_4$ 395.1965, found 395.1952.

*4.8.2.7. 3-(5-(cis-3-Isopropyl-4-oxo-3,4,4a,5,8,8a-hexahydrophthalazin-1-yl)-2-methoxyphenyl)propiolamide (**20**).* Ester **19** (0.50 g, 1.27 mmol) was dissolved in a solution of NH_3 in MeOH (7 M, 4 mL, 28.0 mmol) and stirred at rt for 2 h. The reaction mixture was concentrated and the crude product was purified using flash column chromatography (gradient: 0–50% EtOAc/Hept). The product was obtained as a white solid (390 mg, 84%).

LC-MS (ESI): t_R = 4.19 min, area: > 98%, m/z: 366 $[M+H]^+$.

^{1}H NMR (500 MHz, DMSO-d_6): δ 8.14 (s, 1H), 8.01–7.91 (m, 2H), 7.69 (s, 1H), 7.20 (d, J = 8.8 Hz, 1H), 5.75–5.57 (m, 2H), 4.88 (p, J = 6.6 Hz, 1H), 3.90 (s, 3H), 3.45 (dt, J = 11.6, 5.7 Hz, 1H), 2.81 (t, J = 6.0 Hz, 1H), 2.78–2.68 (m, 1H), 2.25–1.99 (m, 2H), 1.80 (t, J = 14.8 Hz, 1H), 1.24 (d, J = 6.4 Hz, 4H), 1.14 (d, J = 6.7 Hz, 3H).

^{13}C NMR (126 MHz, DMSO-d_6): δ 166.5, 161.7, 154.4, 153.1, 131.6, 129.9, 127.8, 126.3, 124.4, 112.3, 109.7, 88.5, 80.0, 56.6, 46.2, 34.2, 30.3, 22.9, 22.3, 20.9, 20.6.

HRMS (ESI): m/z: $[M+H]^+$ calcd. for $C_{21}H_{24}N_3O_3$ 366.1812, found 366.1797.

4.8.2.8. General procedure for alkynamide synthesis. To a N_2-purged solution of **19** (1 equiv.) in DCM (4 mL per equiv. of **19**) was added K_2CO_3 (5 equiv.) and the corresponding amine (2.5 equiv.) (3 equiv. of Et_3N was added for HCl salts). $AlMe_3$ (2.5 equiv.) was slowly added and the reaction mixture was stirred at rt overnight. The reaction mixture was carefully poured in 1 M aq. HCl (100 mL) and extracted with EtOAc (100 mL). The organic phase was washed with brine (100 mL), dried over $MgSO_4$, filtered and concentrated to obtain the crude product as a brown solid. The crude product was purified using flash column chromatography.

*4.8.2.9. N-Butyl-3-(5-(cis-3-isopropyl-4-oxo-3,4,4a,5,8,8a-hexahydrophthalazin-1-yl)-2-methoxyphenyl)propiolamide (**21**).* This compound was synthesized according to the general procedure using **19** (0.25 g, 0.63 mmol) and butan-1-amine as the corresponding amine. Column chromatography was performed using EtOAc/*n*-hept (gradient: 0–50%) to obtain a white solid (182 mg, 68%).

LC-MS (ESI): t_R = 4.97 min, area: > 98%, m/z: 422 $[M+H]^+$.

^{1}H NMR (500 MHz, $CDCl_3$): δ 7.94 (d, J = 2.4 Hz, 1H), 7.90 (dd, J = 8.8, 2.4 Hz, 1H), 6.96 (t, J = 8.1 Hz, 1H), 6.12–5.87 (m, 1H), 5.84–5.64 (m, 2H), 5.05 (hept, J = 6.7 Hz, 1H), 3.95 (s, 3H), 3.38 (q, J = 6.9 Hz, 2H), 3.27 (dt, J = 11.5, 5.7 Hz, 1H), 3.07–2.96 (m, 1H), 2.74 (t, J = 5.8 Hz, 1H), 2.28–2.10 (m, 2H), 2.09–1.94 (m, 1H), 1.57 (p, J = 7.3 Hz, 2H), 1.41 (hept, J = 7.6 Hz, 2H), 1.36–1.15 (m, 7H), 0.96 (t, J = 7.3 Hz, 3H), 0.89 (t, J = 6.9 Hz, 1H).

^{13}C NMR (126 MHz, $CDCl_3$): δ 166.4, 161.7, 153.4, 152.4, 132.0, 129.4, 129.1, 127.9, 126.0, 123.8, 110.9, 109.8, 87.3, 80.6, 56.1, 46.7, 43.2, 39.7, 34.7, 32.8, 31.4, 31.0, 23.0, 22.3, 20.6, 20.2, 20.1, 13.8.

HRMS (ESI): m/z: $[M+H]^+$ calcd. for $C_{25}H_{32}N_3O_3$ 422.2438, found 422.2428.

*4.8.2.10. N-(Cyclopropylmethyl)-3-(5-(cis-3-isopropyl-4-oxo-3,4,4a,5,-8,8a-hexahydrophthalazin-1-yl)-2-methoxyphenyl)propiolamide (**22**).* This compound was synthesized according to the general procedure using **19** (0.20 g, 0.51 mmol) and cyclopropylmethanamine as the corresponding amine. Column chromatography was performed using EtOAc/*n*-hept (gradient: 0–50%) to obtain a white solid (105 mg, 49%).

LC-MS (ESI): t_R = 4.80 min, area: 98%, m/z: 420 $[M+H]^+$.

^{1}H NMR (500 MHz, $CDCl_3$): δ 8.01–7.85 (m, 2H), 6.95 (dd, J = 8.9, 4.9 Hz, 1H), 6.35–6.18 (m, 1H), 5.82–5.61 (m, 2H), 5.03 (hept, J = 6.7 Hz, 1H), 3.94 (s, 3H), 3.49–3.16 (m, 3H), 3.04–2.94 (m, 1H), 2.72 (t, J = 5.8 Hz, 1H), 2.26–2.09 (m, 2H), 2.07–1.92 (m, 1H), 1.32 (d, J = 6.6 Hz, 3H), 1.19 (d, J = 6.7 Hz, 3H), 1.08–0.95 (m, 1H), 0.61–0.47 (m, 2H), 0.36–0.19 (m, 2H).

^{13}C NMR (126 MHz, $CDCl_3$): δ 166.4, 161.7, 153.3, 152.4, 132.0, 129.1, 128.0, 126.0, 123.8, 110.9, 109.8, 87.3, 80.8, 56.1, 48.3, 46.7, 44.8, 34.7, 31.0, 23.0, 22.3, 20.6, 20.2, 10.5, 3.6.

HRMS (ESI): m/z: $[M+H]^+$ calcd. for $C_{25}H_{30}N_3O_3$ 420.2282, found 420.2277.

*4.8.2.11. N-(Cyclobutylmethyl)-3-(5-(cis-3-isopropyl-4-oxo-3,4,4a,5,8,-8a-hexahydrophthalazin-1-yl)-2-methoxyphenyl)propiolamide (**23**).* This compound was synthesized according to the general procedure using **19** (0.20 g, 0.51 mmol) and cyclobutylmethanamine as the corresponding amine. Column chromatography was performed using EtOAc/*n*-hept (gradient: 0–50%) to obtain a white solid (115 mg, 52%).

LC-MS (ESI): t_R = 5.11 min, area: > 98%, m/z: 434 $[M+H]^+$.

^{1}H NMR (500 MHz, $CDCl_3$): δ 8.05–7.84 (m, 2H), 6.96 (t, J = 9.3 Hz, 1H), 6.08 (q, J = 6.5, 6.0 Hz, 1H), 5.83–5.63 (m, 2H), 5.04 (hept, J = 6.6 Hz, 1H), 3.94 (s, 3H), 3.40 (dd, J = 7.3, 5.9 Hz, 2H), 3.33–3.21 (m, 1H), 3.08–2.94 (m, 1H), 2.73 (q, J = 6.0 Hz, 1H), 2.63–2.46 (m, J = 7.7 Hz, 1H), 2.28–1.65 (m, 10*H*), 1.32 (d, J = 6.6 Hz, 3H), 1.20 (d, J = 6.7 Hz, 3H).

^{13}C NMR (126 MHz, $CDCl_3$): δ 166.4, 161.7, 153.5, 152.4, 132.0, 129.1, 127.9, 126.0, 123.8, 110.9, 109.8, 87.3, 80.8, 56.1, 46.7, 45.2, 35.8, 34.7, 31.0, 25.7, 23.0, 22.3, 20.6, 20.2, 18.3.

HRMS (ESI): m/z: $[M+H]^+$ calcd. for $C_{26}H_{32}N_3O_3$ 434.2438, found 434.2428.

*4.8.2.12. N-(2-Cyanoethyl)-3-(5-(cis-3-isopropyl-4-oxo-3,4,4a,5,8,8a-hexahydrophthalazin-1-yl)-2-methoxyphenyl)propiolamide (**24**).* This compound was synthesized according to the general procedure using **19** (0.20 g, 0.51 mmol) and 3-aminopropanenitrile as the corresponding amine. Column chromatography was performed using EtOAc/*n*-hept (gradient: 0–50%) to obtain a white solid (47 mg, 22%).

LC-MS (ESI): t_R = 4.35 min, area: > 98%, m/z: 419 $[M+H]^+$.

^{1}H NMR (500 MHz, DMSO-d_6): δ 9.12 (t, J = 5.8 Hz, 1H), 8.04–7.93 (m, 2H), 7.21 (d, J = 8.9 Hz, 1H), 5.74–5.57 (m, 2H), 4.88 (hept, J = 6.6 Hz, 1H), 3.91 (s, 3H), 3.46 (dt, J = 11.6, 5.7 Hz, 1H), 3.39 (d, J = 6.3 Hz, 1H), 2.80 (t, J = 6.4 Hz, 1H), 2.77–2.67 (m, 3H), 2.21–2.05 (m, 2H), 1.87–1.73 (m, 1H), 1.24 (d, J = 6.5 Hz, 3H), 1.14 (d, J = 6.7 Hz, 3H).

^{13}C NMR (126 MHz, DMSO-d_6): δ 166.5, 161.8, 153.1, 153.0, 131.7, 130.1, 127.9, 126.3, 124.4, 119.7, 112.4, 109.3, 87.8, 80.8, 56.6, 46.2, 35.6, 34.2, 30.3, 22.8, 22.3, 20.9, 20.6, 17.8.

HRMS (ESI): m/z: $[M+H]^+$ calcd. for $C_{24}H_{27}N_4O_3$ 419.2078, found 419.2065.

4.8.2.13. 1-(3-(5-(cis-3-Isopropyl-4-oxo-3,4,4a,5,8,8a-hexahydrophthalazin-1-yl)-2-methoxyphenyl)propioloyl)azetidine-3-carbonitrile ***(25)***. This compound was synthesized according to the general procedure using **19** (0.20 g, 0.51 mmol) and azetidine-3-carbonitrile. HCl as the corresponding amine. Column chromatography was performed using EtOAc/*n*-hept (gradient: 0–50%) to obtain a white solid (126 mg, 58%).

LC-MS (ESI): t_R = 4.59 min, area: > 98%, m/z: 431 $[M+H]^+$.

^{1}H NMR (500 MHz, $CDCl_3$): δ 7.98–7.87 (m, 2H), 6.97 (d, J = 8.8 Hz, 1H), 5.83–5.63 (m, 2H), 5.04 (hept, J = 6.6 Hz, 1H), 4.67–4.52 (m, 2H), 4.43 (t, J = 9.7 Hz, 1H), 4.34 (dd, J = 10.2, 6.2 Hz, 1H), 3.95 (s, 3H), 3.60 (tt, J = 9.1, 6.2 Hz, 1H), 3.26 (dt, J = 11.5, 5.8 Hz, 1H), 3.05–2.96 (m, 1H), 2.74 (t, J = 6.0 Hz, 1H), 2.26–2.10 (m, 2H), 2.04–1.96 (m, 1H), 1.32 (d, J = 6.6 Hz, 3H), 1.20 (d, J = 6.7 Hz, 3H).

^{13}C NMR (126 MHz, $CDCl_3$): δ 166.4, 162.0, 154.1, 152.2, 131.8, 129.7, 128.0, 126.0, 123.8, 119.0, 110.9, 109.3, 87.5, 83.5, 56.2, 53.4, 51.7, 46.7, 34.7, 31.0, 23.0, 22.3, 20.6, 20.2, 17.5.

HRMS (ESI): m/z: $[M+H]^+$ calcd. for $C_{25}H_{27}N_4O_3$ 431.2078, found 431.2073

4.8.2.14. 3-(5-(cis-3-Isopropyl-4-oxo-3,4,4a,5,8,8a-hexahydrophthalazin-1-yl)-2-methoxyphenyl)-N-((tetrahydrofuran-2-yl)methyl)propiolamide ***(26)***. This compound was synthesized according to the general procedure using **19** (0.20 g, 0.51 mmol) and (tetrahydrofuran-2-yl) methanamine.HCl as the corresponding amine. Column chromatography was performed using EtOAc/*n*-hept (gradient: 0–50%) to obtain a white solid (120 mg, 53%).

LC-MS (ESI): t_R = 4.46 min, area: > 98%, m/z: 450 $[M+H]^+$.

^{1}H NMR (500 MHz, $CDCl_3$): δ 8.05–7.83 (m, 2H), 6.95 (t, J = 8.9 Hz, 1H), 6.43 (t, J = 6.0 Hz, 1H), 5.83–5.61 (m, 2H), 5.03 (hept, J = 6.7 Hz, 1H), 3.98–3.87 (m, 4H), 3.84 (dd, J = 8.8, 6.9 Hz, 1H), 3.75 (q, J = 7.8 Hz, 1H), 3.65–3.54 (m, 1H), 3.38 (q, J = 6.5 Hz, 2H), 3.26 (dt, J = 11.5, 5.7 Hz, 1H), 3.05–2.94 (m, 1H), 2.72 (t, J = 6.0 Hz, 1H), 2.61–2.50 (m, 1H), 2.25–2.05 (m, 3H), 2.04–1.93 (m, 1H), 1.71–1.59 (m, 1H), 1.31 (d, J = 6.6 Hz, 3H), 1.19 (d, J = 6.7 Hz, 3H).

^{13}C NMR (126 MHz, $CDCl_3$): δ 166.4, 161.7, 153.7, 152.4, 132.0, 129.2, 127.9, 126.0, 123.8, 110.9, 109.7, 87.1, 81.2, 77.4, 77.1, 71.3, 67.8, 56.1, 46.7, 42.7, 38.9, 34.7, 30.9, 29.9, 23.0, 22.3, 20.6, 20.2.

HRMS (ESI): m/z: $[M+H]^+$ calcd. for $C_{26}H_{32}N_3O_4$ 450.2387, found 450.2387.

4.8.2.15. Cis-2-Isopropyl-4-(4-methoxy-3-(3-morpholino-3-oxoprop-1-yn-1-yl)phenyl)-4a,5,8,8a-tetrahydrophthalazin-1(2H)-one ***(27)***. This compound was synthesized according to the general procedure using **19** (0.10 g, 0.25 mmol) and morpholine as the corresponding amine. Column chromatography was performed using EtOAc/*n*-hept (gradient: 0–50%) to obtain a white solid (56 mg, 51%).

LC-MS (ESI): t_R = 4.56 min, area: > 98%, m/z: 436 $[M+H]^+$.

^{1}H NMR (500 MHz, $CDCl_3$): δ 7.96 (d, J = 2.2 Hz, 1H), 7.91 (dd, J = 8.8, 2.3 Hz, 1H), 6.96 (d, J = 8.9 Hz, 1H), 5.84–5.61 (m, 2H), 5.04 (hept, J = 6.7 Hz, 1H), 3.94 (d, J = 3.4 Hz, 5H), 3.82–3.75 (m, 2H), 3.72 (s, 4H), 3.27 (dt, J = 11.5, 5.7 Hz, 1H), 3.07–2.94 (m, 1H), 2.74 (t, J = 6.0 Hz, 1H), 2.28–2.09 (m, 2H), 2.05–1.94 (m, 1H), 1.33 (d, J = 6.6 Hz, 3H), 1.21 (d, J = 6.7 Hz, 3H).

^{13}C NMR (126 MHz, $CDCl_3$): δ 166.4, 161.9, 153.3, 152.3, 131.8, 129.3, 128.0, 126.0, 123.8, 110.9, 109.9, 87.3, 85.2, 67.0, 66.5, 56.1, 47.3, 46.7, 42.0, 34.7, 31.0, 23.0, 22.3, 20.6, 20.2.

HRMS (ESI): m/z: $[M+H]^+$ calcd. for $C_{25}H_{30}N_3O_4$ 436.2231, found 436.2217.

4.8.2.16. 3-(5-(cis-3-Isopropyl-4-oxo-3,4,4a,5,8,8a-hexahydrophthalazin-1-yl)-2-methoxyphenyl)-N-(2-methyl-2H-1,2,3-triazol-4-yl)propiolamide ***(11)***. This compound was synthesized according to the general procedure using **19** (0.10 g, 0.25 mmol) and 2-methyl-2*H*-1,2,3-triazol-4-amine.HCl as the corresponding amine. Column chromatography was performed using EtOAc/*n*-hept (gradient: 10–80%) to obtain a white solid (42 mg, 37%).

LC-MS (ESI): t_R = 4.54 min, area: > 97%, m/z: 447 $[M+H]^+$.

^{1}H NMR (500 MHz, $CDCl_3$): δ 8.33 (s, 1H), 7.94 (s, 1H), 7.91 (d, J = 2.3 Hz, 1H), 7.86 (dd, J = 8.8, 2.4 Hz, 1H), 6.90 (d, J = 8.9 Hz, 1H), 5.78–5.57 (m, 2H), 4.98 (hept, J = 6.7 Hz, 1H), 4.06 (s, 3H), 3.89 (s, 3H), 3.26–3.15 (m, 1H), 2.99–2.89 (m, 1H), 2.68 (t, J = 6.0 Hz, 1H), 2.20–2.04 (m, 2H), 2.01–1.89 (m, 1H), 1.26 (d, J = 6.6 Hz, 3H), 1.14 (d, J = 6.7 Hz, 3H).

^{13}C NMR (126 MHz, $CDCl_3$): δ 166.4, 162.0, 152.2, 149.8, 143.2, 132.2, 129.7, 128.1, 126.0, 125.4, 123.8, 111.0, 109.2, 86.5, 83.4, 56.4, 46.8, 41.7, 34.7, 31.0, 23.0, 22.3, 20.6, 20.2.

HRMS (ESI): m/z: $[M+H]^+$ calcd. for $C_{24}H_{27}N_6O_3$ 447.2139, found 447.2131.

4.8.2.17. N-(1-(3-Cyanopropyl)-1H-pyrazol-3-yl)-3-(5-(cis-3-isopropyl-4-oxo-3,4,4a,5,8,8a-hexahydrophthalazin-1-yl)-2-methoxyphenyl) propiolamide ***(12)***. This compound was synthesized according to the general procedure using **19** (0.10 g, 0.25 mmol) and 4-(3-amino-1*H*-pyrazol-1-yl)butanenitrile as the corresponding amine. Column chromatography was performed using EtOAc/*n*-hept (gradient: 10–80%) to obtain a white solid (11 mg, 9%).

LC-MS (ESI): t_R = 4.49 min, area: > 98%, m/z: 499 $[M+H]^+$.

^{1}H NMR (500 MHz, $CDCl_3$): δ 8.29 (s, 1H), 7.99 (d, J = 2.3 Hz, 1H), 7.93 (dd, J = 8.8, 2.3 Hz, 1H), 7.37 (s, 1H), 6.98 (d, J = 8.8 Hz, 1H), 6.76 (s, 1H), 5.85–5.66 (m, 2H), 5.06 (hept, J = 6.6 Hz, 1H), 4.20 (t, J = 6.2 Hz, 2H), 3.97 (s, 3H), 3.33–3.25 (m, 1H), 3.07–2.98 (m, 1H), 2.76 (t, J = 5.9 Hz, 1H), 2.35 (t, J = 6.8 Hz, 2H), 2.28–2.13 (m, 4H), 2.08–1.97 (m, 1H), 1.35 (d, J = 6.6 Hz, 3H), 1.23 (d, J = 6.7 Hz, 3H).

^{13}C NMR (126 MHz, $CDCl_3$): δ 166.4, 162.0, 152.3, 150.0, 132.2, 131.0, 129.5, 128.0, 126.0, 123.8, 118.6, 111.0, 109.4, 98.2, 87.0, 82.6, 56.1, 49.9, 46.8, 34.7, 31.0, 25.9, 23.0, 22.3, 20.6, 20.2, 14.5.

HRMS (ESI): m/z: $[M+H]^+$ calcd. for $C_{28}H_{31}N_6O_3$ 499.2452, found 499.2449.

4.8.2.18. N-(Furan-2-ylmethyl)-3-(5-(cis-3-isopropyl-4-oxo-3,4,4a,5,8,-8a-hexahydrophthalazin-1-yl)-2-methoxyphenyl)propiolamide ***(28)***. This compound was synthesized according to the general procedure using **19** (0.20 g, 0.51 mmol) and furfurylamine as the corresponding amine. Column chromatography was performed using EtOAc/*n*-hept (gradient: 0–50%) to obtain a white solid (112 mg, 50%).

LC-MS (ESI): t_R = 4.78 min, area: > 98%, m/z: 446 $[M+H]^+$.

^{1}H NMR (500 MHz, $CDCl_3$): δ 8.02–7.85 (m, 2H), 7.39 (d, J = 1.8 Hz, 1H), 7.01–6.91 (m, 1H), 6.42 (d, J = 6.8 Hz, 1H), 6.38–6.27 (m, 2H), 5.85–5.61 (m, 2H), 5.05 (p, J = 6.6 Hz, 1H), 4.55 (d, J = 5.6 Hz, 2H), 3.93 (s, 3H), 3.26 (dt, J = 11.5, 5.7 Hz, 1H), 3.11–2.91 (m, 1H), 2.73 (t, J = 6.0 Hz, 1H), 2.27–2.10 (m, 2H), 2.04–1.95 (m, 1H), 1.33 (d, J = 6.6 Hz, 3H), 1.20 (d, J = 6.7 Hz, 3H).

^{13}C NMR (126 MHz, $CDCl_3$): δ 166.4, 161.8, 153.1, 152.4, 150.3, 142.5, 132.0, 129.3, 127.9, 126.0, 123.8, 110.9, 110.6, 109.6, 108.1, 86.8, 81.5, 56.1, 46.7, 36.7, 34.7, 31.0, 23.0, 22.3, 20.6, 20.2.

HRMS (ESI): m/z: $[M+H]^+$ calcd. for $C_{26}H_{28}N_3O_4$ 446.2074, found 446.2055.

*4.8.2.19. 3-(5-(cis-3-Isopropyl-4-oxo-3,4,4a,5,8,8a-hexahydrophthalazin-1-yl)-2-methoxyphenyl)-N-((5-methylfuran-2-yl)methyl)propiolamide **(29)***. This compound was synthesized according to the general procedure using **19** (0.20 g, 0.51 mmol) and (5-methylfuran-2-yl) methanamine as the corresponding amine. Column chromatography was performed using EtOAc/*n*-hept (gradient: 0–50%) to obtain a white solid (112 mg, 48%).

LC-MS (ESI): t_R = 4.96 min, area: > 98%, *m/z*: 460 $[M+H]^+$.

^{1}H NMR (500 MHz, DMSO-d_6): δ 9.21 (t, J = 5.8 Hz, 1H), 8.02–7.93 (m, 2H), 7.20 (d, J = 8.8 Hz, 1H), 6.15 (d, J = 3.0 Hz, 1H), 6.03–5.97 (m, 1H), 5.74–5.58 (m, 2H), 4.87 (hept, J = 6.6 Hz, 1H), 4.27 (d, J = 5.7 Hz, 2H), 3.90 (s, 3H), 3.44 (dt, J = 11.6, 5.8 Hz, 1H), 2.80 (t, J = 6.0 Hz, 1H), 2.78–2.69 (m, 1H), 2.23 (d, J = 1.0 Hz, 3H), 2.19–2.04 (m, 2H), 1.85–1.74 (m, 1H), 1.23 (d, J = 6.5 Hz, 3H), 1.14 (d, J = 6.8 Hz, 3H).

^{13}C NMR (126 MHz, DMSO-d_6): δ 166.5, 161.8, 153.1, 152.6, 151.3, 145.0, 131.6, 130.0, 127.9, 126.3, 124.4, 112.3, 109.5, 108.7, 106.9, 88.0, 80.7, 56.6, 46.2, 36.1, 34.2, 30.3, 22.9, 22.3, 20.9, 20.6, 13.8.

HRMS (ESI): *m/z*: $[M+H]^+$ calcd. for $C_{27}H_{30}N_3O_4$ 460.2231, found 460.2216.

*4.8.2.20. 3-(5-(cis-3-Isopropyl-4-oxo-3,4,4a,5,8,8a-hexahydrophthalazin-1-yl)-2-methoxyphenyl)-N-(thiophen-2-ylmethyl)propiolamide **(30)***. This compound was synthesized according to the general procedure using **19** (0.15 g, 0.38 mmol) and thiophen-2-ylmethanamine as the corresponding amine. Column chromatography was performed using EtOAc/*n*-hept (gradient: 0–50%) to obtain a white solid (76 mg, 43%).

LC-MS (ESI): t_R = 5.00 min, area: > 98%, *m/z*: 462 $[M+H]^+$.

^{1}H NMR (500 MHz, $CDCl_3$): δ 7.92 (d, J = 2.4 Hz, 1H), 7.89 (dd, J = 8.8, 2.4 Hz, 1H), 7.27–7.23 (m, 1H), 7.08–7.02 (m, 1H), 6.97 (dd, J = 5.2, 3.4 Hz, 1H), 6.94 (d, J = 8.9 Hz, 1H), 6.54 (t, J = 5.8 Hz, 1H), 5.82–5.64 (m, 2H), 5.03 (p, J = 6.6 Hz, 1H), 4.71 (d, J = 5.7 Hz, 2H), 3.91 (s, 3H), 3.25 (dt, J = 11.4, 5.7 Hz, 1H), 3.04–2.95 (m, 1H), 2.71 (t, J = 6.0 Hz, 1H), 2.24–2.10 (m, 2H), 2.04–1.93 (m, 1H), 1.32 (d, J = 6.5 Hz, 3H), 1.19 (d, J = 6.7 Hz, 3H).

^{13}C NMR (126 MHz, $CDCl_3$): δ 166.4, 161.8, 153.0, 152.4, 139.6, 132.0, 129.3, 127.9, 127.0, 126.7, 126.0, 125.6, 123.8, 110.9, 109.6, 86.9, 81.6, 56.1, 46.7, 38.5, 34.7, 30.9, 23.0, 22.3, 20.6, 20.2.

HRMS (ESI): *m/z*: $[M+H]^+$ calcd. for $C_{26}H_{28}N_3O_3S$ 462.1846, found 462.1836.

*4.8.2.21. 3-(5-(cis-3-Isopropyl-4-oxo-3,4,4a,5,8,8a-hexahydrophthalazin-1-yl)-2-methoxyphenyl)-N-(2-(thiophen-2-yl)ethyl)propiolamide **(31)***. This compound was synthesized according to the general procedure using **19** (0.15 g, 0.38 mmol) and 2-(thiophen-2-yl) ethanamine as the corresponding amine. Column chromatography was performed using EtOAc/*n*-hept (gradient: 0–50%) to obtain a white solid (87 mg, 48%).

LC-MS (ESI): t_R = 5.09 min, area: > 98%, *m/z*: 476 $[M+H]^+$.

^{1}H NMR (500 MHz, $CDCl_3$): δ 7.92 (d, J = 2.4 Hz, 1H), 7.88 (dd, J = 8.8, 2.4 Hz, 1H), 7.21–7.14 (m, 1H), 6.99–6.91 (m, 2H), 6.88 (dd, J = 3.3, 1.2 Hz, 1H), 6.36 (t, J = 6.1 Hz, 1H), 5.81–5.62 (m, 2H), 5.04 (p, J = 6.6 Hz, 1H), 3.91 (s, 3H), 3.64 (q, J = 6.6 Hz, 2H), 3.25 (dt, J = 11.5, 5.7 Hz, 1H), 3.10 (t, J = 6.8 Hz, 2H), 3.05–2.95 (m, 1H), 2.72 (q, J = 7.7, 5.9 Hz, 1H), 2.25–1.97 (m, 3H), 1.32 (dd, J = 6.6, 2.6 Hz, 3H), 1.20 (dd, J = 6.7, 2.9 Hz, 3H).

^{13}C NMR (126 MHz, $CDCl_3$): δ 166.4, 161.8, 153.4, 152.4, 140.9, 132.0, 129.2, 127.9, 127.1, 126.0, 125.5, 124.1, 123.8, 110.9, 109.7, 87.2, 81.1, 56.1, 46.7, 41.3, 34.7, 30.9, 26.9, 23.0, 22.3, 20.6, 20.2.

HRMS (ESI): *m/z*: $[M+H]^+$ calcd. for $C_{27}H_{30}N_3O_3S$ 476.2002, found 476.1990.

*4.8.2.22. 3-(5-(cis-3-Isopropyl-4-oxo-3,4,4a,5,8,8a-hexahydrophthalazin-1-yl)-2-methoxyphenyl)-N-((2-methylthiazol-4-yl)methyl)propiolamide **(32)***. This compound was synthesized according to the general procedure using **19** (0.20 g, 0.51 mmol) and (2-methylthiazol-4-yl) methanamine.2HCl as the corresponding amine. Column chromatography was performed using EtOAc/*n*-hept (gradient: 0–50%) to obtain a white solid (142 mg, 59%).

LC-MS (ESI): t_R = 4.57 min, area: > 97%, *m/z*: 477 $[M+H]^+$.

^{1}H NMR (500 MHz, DMSO-d_6): δ 9.29 (t, J = 6.0 Hz, 1H), 8.03–7.91 (m, 2H), 7.25 (d, J = 0.9 Hz, 1H), 7.21 (d, J = 8.8 Hz, 1H), 5.73–5.57 (m, 2H), 4.88 (p, J = 6.6 Hz, 1H), 4.37 (dd, J = 6.0, 1.0 Hz, 2H), 3.91 (s, 3H), 3.44 (dt, J = 11.7, 5.8 Hz, 1H), 2.81 (t, J = 6.1 Hz, 1H), 2.77–2.68 (m, 1H), 2.63 (s, 3H), 2.21–2.05 (m, 2H), 1.87–1.71 (m, 1H), 1.24 (d, J = 6.6 Hz, 3H), 1.14 (d, J = 6.7 Hz, 3H).

^{13}C NMR (126 MHz, DMSO-d_6): δ 166.5, 166.0, 161.8, 153.1, 152.9, 152.7, 131.6, 130.0, 127.9, 126.3, 124.4, 115.6, 112.4, 109.6, 88.1, 80.6, 56.6, 46.2, 34.2, 30.3, 22.9, 22.3, 20.9, 20.6, 19.2.

HRMS (ESI): *m/z*: $[M+H]^+$ calcd. for $C_{26}H_{29}N_4O_3S$ 477.1955, found 477.1939.

*4.8.2.23. 3-(5-(cis-3-Isopropyl-4-oxo-3,4,4a,5,8,8a-hexahydrophthalazin-1-yl)-2-methoxyphenyl)-N-(2-(thiazol-2-yl)ethyl)propiolamide **(33)***. This compound was synthesized according to the general procedure using **19** (0.15 g, 0.38 mmol) and 2-(thiazol-2-yl)ethanamine as the corresponding amine. Column chromatography was performed using EtOAc/*n*-hept (gradient: 0–50%) to obtain a white solid (81 mg, 45%).

LC-MS (ESI): t_R = 4.59 min, area: > 98%, *m/z*: 477 $[M+H]^+$.

^{1}H NMR (500 MHz, $CDCl_3$): δ 7.93 (d, J = 2.3 Hz, 1H), 7.89 (dd, J = 8.8, 2.4 Hz, 1H), 7.74 (d, J = 3.3 Hz, 1H), 6.94 (d, J = 8.8 Hz, 1H), 6.91 (t, J = 6.1 Hz, 1H), 5.83–5.64 (m, 2H), 5.05 (hept, J = 6.6 Hz, 1H), 3.94 (s, 3H), 3.85 (q, J = 6.1 Hz, 2H), 3.34–3.23 (m, 3H), 3.06–2.96 (m, 1H), 2.73 (t, J = 6.0 Hz, 1H), 2.27–2.11 (m, 2H), 2.06–1.97 (m, 1H), 1.33 (d, J = 6.7 Hz, 3H), 1.21 (d, J = 6.6 Hz, 3H).

^{13}C NMR (126 MHz, $CDCl_3$): δ 167.7, 166.4, 161.8, 153.4, 152.4, 142.4, 132.0, 129.2, 127.9, 126.0, 123.8, 119.0, 110.9, 109.8, 87.2, 81.2, 56.1, 46.7, 38.7, 34.7, 32.3, 31.0, 23.0, 22.3, 20.6, 20.2.

HRMS (ESI): *m/z*: $[M+H]^+$ calcd. for $C_{26}H_{29}N_4O_3S$ 477.1955, found 477.1941.

*4.8.2.24. N-((2,4-Dimethylthiazol-5-yl)methyl)-3-(5-(cis-3-isopropyl-4-oxo-3,4,4a,5,8,8a-hexahydrophthalazin-1-yl)-2-methoxyphenyl) propiolamide **(34)***. This compound was synthesized according to the general procedure using **19** (0.10 g, 0.25 mmol) and (2,4-dimethylthiazol-5-yl)methanamine as the corresponding amine. Column chromatography was performed using EtOAc/*n*-hept (gradient: 10–80%) to obtain a white solid (36 mg, 29%).

LC-MS (ESI): t_R = 4.39 min, area: > 98%, *m/z*: 491 $[M+H]^+$.

^{1}H NMR (500 MHz, $CDCl_3$): δ 7.93 (d, J = 2.3 Hz, 1H), 7.90 (dd, J = 8.8, 2.4 Hz, 1H), 6.95 (d, J = 8.8 Hz, 1H), 6.27 (t, J = 5.7 Hz, 1H), 5.83–5.76 (m, 1H), 5.72–5.64 (m, 1H), 5.05 (p, J = 6.7 Hz, 1H), 4.61 (d, J = 5.6 Hz, 2H), 3.94 (s, 3H), 3.30–3.23 (m, 1H), 3.07–2.97 (m, 1H), 2.74 (t, J = 6.1 Hz, 1H), 2.66 (s, 3H), 2.41 (s, 3H), 2.26–2.10 (m, 2H), 2.07–1.95 (m, 1H), 1.33 (d, J = 6.6 Hz, 3H), 1.21 (d, J = 6.7 Hz, 3H).

^{13}C NMR (126 MHz, $CDCl_3$): δ 166.4, 164.5, 161.8, 153.0, 152.3, 149.7, 132.1, 129.4, 128.0, 126.1, 126.0, 123.8, 110.9, 109.5, 86.6, 81.9, 56.1, 46.7, 35.3, 34.7, 31.0, 23.0, 22.3, 20.6, 20.2, 19.1, 14.9.

HRMS (ESI): *m/z*: $[M+H]^+$ calcd. for $C_{27}H_{31}N_4O_3S$ 491.2111, found 491.2102.

*4.8.2.25. 3-(5-(cis-3-Isopropyl-4-oxo-3,4,4a,5,8,8a-hexahydrophthalazin-1-yl)-2-methoxyphenyl)-N-((1-methyl-1H-pyrazol-4-yl)methyl) propiolamide **(35)***. This compound was synthesized according to the general procedure using **19** (0.15 g, 0.38 mmol) and (1-methyl-1*H*-pyrazol-4-yl)methanamine as the corresponding amine. Column chromatography was performed using EtOAc/*n*-hept (gradient: 10–80%) to obtain a white solid (73 mg, 42%).

LC-MS (ESI): t_R = 4.37 min, area: > 98%, *m/z*: 460 $[M+H]^+$.

^{1}H NMR (500 MHz, $CDCl_3$): δ 7.89 (d, J = 2.3 Hz, 1H), 7.86 (dd,

J = 8.8, 2.4 Hz, 1H), 7.40 (d, J = 15.1 Hz, 2H), 6.97–6.89 (m, 1H), 6.61 (t, J = 5.7 Hz, 1H), 5.79–5.58 (m, 2H), 5.00 (p, J = 6.7 Hz, 1H), 4.36 (d, J = 5.7 Hz, 2H), 3.88 (s, 3H), 3.84 (s, 3H), 3.27–3.17 (m, 1H), 3.02–2.91 (m, 1H), 2.69 (t, J = 5.9 Hz, 1H), 2.23–2.06 (m, 2H), 2.01–1.90 (m, 1H), 1.29 (d, J = 6.6 Hz, 3H), 1.17 (d, J = 6.7 Hz, 3H).

^{13}C NMR (126 MHz, $CDCl_3$): δ 166.4, 161.7, 153.2, 152.4, 138.8, 131.9, 129.7, 129.2, 127.9, 126.0, 123.8, 117.7, 110.9, 109.7, 87.1, 81.2, 56.0, 46.7, 38.9, 34.6, 34.3, 30.9, 22.9, 22.2, 20.6, 20.2.

HRMS (ESI): m/z: $[M+H]^+$ calcd. for $C_{26}H_{30}N_5O_3$ 460.2343, found 460.2337.

4.8.2.26. N-(3-(1H-Imidazol-1-yl)propyl)-3-(5-(cis-3-isopropyl-4-oxo-3,-4,4a,5,8,8a-hexahydrophthalazin-1-yl)-2-methoxyphenyl)propiolamide ***(36)***. This compound was synthesized according to the general procedure using **19** (0.15 g, 0.38 mmol) and 3-(1*H*-imidazol-1-yl) propan-1-amine as the corresponding amine. Column chromatography was performed using EtOAc/*n*-hept (gradient: 10–100%)to obtain a white solid (101 mg, 56%).

LC-MS (ESI): t_R = 3.59 min, area: > 98%, m/z: 474 $[M+H]^+$.

^{1}H NMR (500 MHz, $CDCl_3$): δ 7.86 (d, J = 2.4 Hz, 1H), 7.82 (dd, J = 8.8, 2.3 Hz, 1H), 7.45 (s, 1H), 7.08 (t, J = 6.2 Hz, 1H), 7.01 (s, 1H), 6.93–6.84 (m, 2H), 5.75–5.54 (m, 2H), 4.96 (p, J = 6.7 Hz, 1H), 3.97 (t, J = 6.9 Hz, 2H), 3.85 (s, 3H), 3.27 (q, J = 6.5 Hz, 2H), 3.23–3.14 (m, 1H), 2.97–2.86 (m, 1H), 2.65 (t, J = 6.0 Hz, 1H), 2.19–2.03 (m, 2H), 2.03–1.97 (m, 2H), 1.96–1.86 (m, 1H), 1.24 (d, J = 6.6 Hz, 3H), 1.17–1.09 (m, 3H).

^{13}C NMR (126 MHz, $CDCl_3$): δ 166.4, 161.7, 153.9, 152.4, 137.2, 132.0, 129.4, 129.3, 128.0, 126.0, 123.8, 118.9, 111.0, 109.7, 87.1, 81.3, 56.1, 46.7, 44.4, 36.9, 34.7, 30.9, 30.9, 23.0, 22.3, 20.6, 20.2.

HRMS (ESI): m/z: $[M+H]^+$ calcd. for $C_{27}H_{32}N_5O_3$ 474.2500, found 474.2496.

4.8.2.27. N-Benzyl-3-(5-(cis-3-isopropyl-4-oxo-3,4,4a,5,8,8a-hexahydrophthalazin-1-yl)-2-methoxyphenyl)propiolamide ***(37)***. This compound was synthesized according to the general procedure using **19** (0.10 g, 0.25 mmol) and phenylmethanamine as the corresponding amine. Column chromatography was performed using EtOAc/*n*-hept (gradient: 0–50%) to obtain a white solid (80 mg, 69%).

LC-MS (ESI): t_R = 4.93 min, area: > 98%, m/z: 456 $[M+H]^+$.

^{1}H NMR (500 MHz, $CDCl_3$): δ 7.94 (d, J = 2.2 Hz, 1H), 7.90 (dd, J = 8.8, 2.3 Hz, 1H), 7.41–7.29 (m, 5H), 6.94 (d, J = 8.8 Hz, 1H), 6.41 (t, J = 5.8 Hz, 1H), 5.83–5.63 (m, 2H), 5.04 (hept, J = 6.7 Hz, 1H), 4.56 (d, J = 5.7 Hz, 2H), 3.92 (s, 3H), 3.26 (dt, J = 11.5, 5.7 Hz, 1H), 3.06–2.95 (m, 1H), 2.72 (t, J = 5.9 Hz, 1H), 2.26–2.10 (m, 2H), 2.07–1.95 (m, 1H), 1.33 (d, J = 6.5 Hz, 3H), 1.20 (d, J = 6.7 Hz, 3H).

^{13}C NMR (126 MHz, $CDCl_3$): δ 166.4, 161.8, 153.3, 152.4, 137.3, 132.0, 129.2, 128.8, 128.1, 127.9, 127.8, 126.0, 123.8, 110.9, 109.7, 87.0, 81.4, 56.1, 46.7, 44.0, 34.7, 31.0, 23.0, 22.3, 20.6, 20.2.

HRMS (ESI): m/z: $[M+H]^+$ calcd. for $C_{28}H_{30}N_3O_3$ 456.2282, found 456.2275.

4.8.2.28. 3-(5-(cis-3-Isopropyl-4-oxo-3,4,4a,5,8,8a-hexahydrophthalazin-1-yl)-2-methoxyphenyl)-N-(pyridin-3-ylmethyl)propiolamide ***(38)***. This compound was synthesized according to the general procedure using **19** (0.20 g, 0.51 mmol) and pyridin-3-ylmethanamine.HCl as the corresponding amine. Column chromatography was performed using EtOAc/*n*-hept (gradient: 0–50%) to obtain a white solid (142 mg, 61%).

LC-MS (ESI): t_R = 3.72 min, area: > 98%, m/z: 457 $[M+H]^+$.

^{1}H NMR (500 MHz, DMSO-d_6): δ 9.37 (t, J = 6.1 Hz, 1H), 8.52 (d, J = 2.2 Hz, 1H), 8.48 (dd, J = 4.7, 1.7 Hz, 1H), 8.02–7.92 (m, 2H), 7.70 (dt, J = 7.8, 2.0 Hz, 1H), 7.43–7.33 (m, 1H), 7.20 (d, J = 8.8 Hz, 1H), 5.75–5.56 (m, 2H), 4.87 (hept, J = 6.6 Hz, 1H), 4.37 (d, J = 6.0 Hz, 2H), 3.90 (s, 3H), 3.44 (dt, J = 11.5, 5.7 Hz, 1H), 2.80 (t, J = 6.1 Hz, 1H), 2.78–2.68 (m, 1H), 2.21–2.05 (m, 2H), 1.86–1.72 (m, 1H), 1.23 (d, J = 6.7 Hz, 3H), 1.13 (d, J = 6.8 Hz, 3H).

^{13}C NMR (126 MHz, DMSO-d_6): δ 166.5, 161.8, 153.1, 152.9, 149.4, 148.8, 135.8, 134.6, 131.6, 130.1, 127.9, 126.3, 124.4, 124.0, 112.3, 109.4, 87.9, 80.8, 56.6, 46.2, 40.6, 34.2, 30.3, 22.8, 22.3, 20.9, 20.5.

HRMS (ESI): m/z: $[M+H]^+$ calcd. for $C_{27}H_{29}N_4O_3$ 457.2234, found 457.2220.

4.8.2.29. 3-(5-(cis-3-Isopropyl-4-oxo-3,4,4a,5,8,8a-hexahydrophthalazin-1-yl)-2-methoxyphenyl)-N-(pyridin-4-ylmethyl)propiolamide ***(39)***. This compound was synthesized according to the general procedure using **19** (0.10 g, 0.25 mmol) and pyridin-4-ylmethanamine as the corresponding amine. Column chromatography was performed using EtOAc/*n*-hept (gradient: 0–50%) to obtain a white solid (67 mg, 58%).

LC-MS (ESI): t_R = 3.64 min, area: > 98%, m/z: 457 $[M+H]^+$.

^{1}H NMR (500 MHz, $CDCl_3$): δ 8.62 (s, 2H), 7.95 (d, J = 2.3 Hz, 1H), 7.91 (dd, J = 8.8, 2.4 Hz, 1H), 7.29 (s, 2H), 6.98–6.90 (m, 1H), 6.67 (t, J = 6.3 Hz, 1H), 5.83–5.64 (m, 2H), 5.05 (hept, J = 6.7 Hz, 1H), 4.58 (d, J = 6.1 Hz, 2H), 3.94 (s, 3H), 3.26 (dq, J = 11.9, 5.9 Hz, 1H), 3.06–2.96 (m, 1H), 2.74 (t, J = 6.0 Hz, 1H), 2.26–2.10 (m, 2H), 2.06–1.99 (m, 1H), 1.33 (d, J = 6.6 Hz, 3H), 1.21 (d, J = 6.6 Hz, 3H).

^{13}C NMR (126 MHz, $CDCl_3$): δ 166.4, 161.8, 153.6, 152.3, 149.9, 146.6, 132.1, 129.7, 129.5, 128.0, 126.0, 123.8, 111.0, 109.4, 86.6, 82.2, 56.1, 46.7, 42.6, 34.7, 31.0, 23.0, 22.3, 20.6, 20.2.

HRMS (ESI): m/z: $[M+H]^+$ calcd. for $C_{27}H_{29}N_4O_3$ 457.2234, found 457.2220.

4.8.2.30. 3-(5-(cis-3-Isopropyl-4-oxo-3,4,4a,5,8,8a-hexahydrophthalazin-1-yl)-2-methoxyphenyl)-N-(3-methoxyphenyl)propiolamide ***(40)***. This compound was synthesized according to the general procedure using **19** (0.20 g, 0.51 mmol) and 3-methoxyaniline as the corresponding amine. Column chromatography was performed using EtOAc/*n*-hept (gradient: 0–50%) to obtain a white solid (98 mg, 41%).

LC-MS (ESI): t_R = 5.10 min, area: > 98%, m/z: 472 $[M+H]^+$.

^{1}H NMR (500 MHz, $CDCl_3$): δ 7.97 (d, J = 2.6 Hz, 2H), 7.92 (dd, J = 8.8, 2.3 Hz, 1H), 7.33 (t, J = 2.3 Hz, 1H), 7.24 (t, J = 8.1 Hz, 1H), 7.09 (dd, J = 7.9, 1.9 Hz, 1H), 6.97 (d, J = 8.9 Hz, 1H), 6.71 (dd, J = 8.2, 2.4 Hz, 1H), 5.85–5.63 (m, 2H), 5.06 (hept, J = 6.6 Hz, 1H), 3.96 (s, 3H), 3.82 (s, 3H), 3.28 (dt, J = 11.6, 5.7 Hz, 1H), 3.07–2.97 (m, 1H), 2.74 (t, J = 6.0 Hz, 1H), 2.27–2.12 (m, 2H), 2.05–1.96 (m, 1H), 1.34 (d, J = 6.6 Hz, 3H), 1.22 (d, J = 6.7 Hz, 3H).

^{13}C NMR (126 MHz, $CDCl_3$): δ 166.4, 161.9, 160.1, 152.4, 151.0, 138.6, 132.1, 129.8, 129.5, 128.0, 126.0, 123.8, 112.1, 111.0, 110.6, 109.5, 105.8, 87.7, 82.0, 56.1, 55.4, 46.8, 34.7, 31.0, 23.0, 22.3, 20.6, 20.2.

HRMS (ESI): m/z: $[M+H]^+$ calcd. for $C_{28}H_{30}N_3O_4$ 472.2231, found 472.2243

4.8.2.31. N-(2-Fluorophenethyl)-3-(5-(cis-3-isopropyl-4-oxo-3,4,4a,5,8,-8a-hexahydrophthalazin-1-yl)-2-methoxyphenyl)propiolamide ***(41)***. This compound was synthesized according to the general procedure using **19** (0.20 g, 0.51 mmol) and 2-(2-fluorophenyl)ethanamine as the corresponding amine. Column chromatography was performed using EtOAc/*n*-hept (gradient: 0–50%) to obtain a white solid (110 mg, 45%).

LC-MS (ESI): t_R = 5.07 min, area: > 98%, m/z: 488 $[M+H]^+$.

^{1}H NMR (500 MHz, $CDCl_3$): δ 8.00–7.84 (m, 2H), 7.27–7.16 (m, 2H), 7.14–6.99 (m, 2H), 6.95 (dd, J = 13.4, 8.9 Hz, 1H), 6.31 (q, J = 7.0 Hz, 1H), 5.85–5.61 (m, 2H), 5.04 (p, J = 6.7 Hz, 1H), 3.91 (s, 3H), 3.62 (q, J = 6.8 Hz, 2H), 3.27 (tt, J = 11.5, 5.7 Hz, 1H), 3.07–2.87 (m, 3H), 2.73 (dt, J = 11.9, 5.9 Hz, 1H), 2.28–2.09 (m, 2H), 2.04–1.94 (m, 1H), 1.32 (dd, J = 6.6, 3.4 Hz, 3H), 1.20 (dd, J = 6.9, 4.2 Hz, 3H).

^{13}C NMR (126 MHz, $CDCl_3$): δ 166.4, 161.8, 153.5, 152.4, 132.0, 131.1, 129.2, 128.4, 127.9, 126.0, 125.4, 124.3, 123.8, 115.5, 115.3, 110.9, 109.8, 87.2, 81.0, 56.1, 46.7, 39.9, 34.7, 30.9, 29.0, 23.0, 22.3, 20.6, 20.2.

HRMS (ESI): m/z: $[M+H]^+$ calcd. for $C_{29}H_{31}FN_3O_3$ 488.2344, found 488.2341.

Declaration of Competing Interest

None.

Acknowledgments

We thank F.G.J. Custers (Vrije Universiteit Amsterdam) for analytical support. We thank Jay Bangs (University at Buffalo) for providing *T. brucei brucei* culture medium, Viacheslav O. Nikolaev (Universitätsklinikum Hamburg-Eppendorf) for providing the Epac1camps plasmid, Tom Seebeck for the anti-PFR antibody. Funding: This work was supported by the European Commission 7th Framework Programme FP7-HEALTH-2013-INNOVATION-1 under project reference 602666 “Parasite-specific cyclic nucleotide phosphodiesterase inhibitors to target Neglected Parasitic Diseases” (PDE4NPD) and by the European Union’s Horizon2020 MSCA Programme under grant agreement 675899 (FRAGNET). This work was supported in part by grant R01GM109984 to NCS.

Author contributions

E.d.H., G.J.S. and I.J.P.d.E. were involved in compound design, synthesis and analysis. A.K.S. and D.G.B. were involved in protein production, crystallization, data collection and refinement for structural studies. E.d.H., A.K.S. and D.G.B. were involved in crystal structure analysis. E.d.H. and A.J.K. were involved in virtual screening and docking. T.v.d.M., P.S., and M.S. were involved in the biochemical assays. G.C. and L.M. were involved in the phenotypic cellular assays. P.B. and A.R.B. were involved in SPR analysis. M.O., NS and DB were involved in the target validation experiments. L.M., G.J.S., I.J.P.d.E., D.G.B. and R.L. supervised the experiments and conceived the project. E.d.H., A.K.S. G.J.S., I.J.P.d.E., and R.L. integrated all data and wrote the manuscript.

Appendix A. Supplementary data

Supplementary data to this article can be found online at https://doi.org/10.1016/j.bmc.2019.06.026.

References

1. Brun R, Blum J, Chappuis F, Burri C. Human african trypanosomiasis. *Lancet.* 2010;375:148–159.
2. Büscher P, Cecchi G, Jamonneau V, Priotto G. Human African trypanosomiasis. *Lancet.* 2017;390:2397–2409.
3. Babokhov P, Sanyaolu AO, Oyibo WA, Fagbenro-Beyioku AF, Iriemenam NC. A current analysis of chemotherapy strategies for the treatment of human African trypanosomiasis. *Pathogens Global Health.* 2013;107:242–252.
4. Kennedy PGE. Human African trypanosomiasis of the CNS: current issues and challenges. *J Clin Invest.* 2004;113:496–504.
5. Baker CH, Welburn SC. The long wait for a new drug for human african trypanosomiasis. *Trends Parasitol.* 2018.
6. Anene BM, Onah DN, Nawa Y. Drug resistance in pathogenic African trypanosomes: what hopes for the future? *Vet Parasitol.* 2001;96:83–100.
7. Baker N, de Koning HP, Maser P, Horn D. Drug resistance in African trypanosomiasis: the melarsoprol and pentamidine story. *Trends Parasitol.* 2013;29:110–118.
8. de Koning HP. Drug resistance in protozoan parasites. *Emerg Top Life Sci.* 2017;1:627.
9. Gould MK, Schnaufer A. Independence from kinetoplast DNA maintenance and expression is associated with multidrug resistance in trypanosoma brucei in vitro. *Antimicrob Agents Chemother.* 2014;58:2925–2928.
10. Sokolova AY, Wyllie S, Patterson S, Oza SL, Read KD, Fairlamb AH. Cross-resistance to nitro drugs and implications for treatment of human African trypanosomiasis. *Antimicrob Agents Chemother.* 2010;54:2893–2900.
11. WHO, Trypanosomiasis, human African (sleeping sickness), https://www.who.int/news-room/fact-sheets/detail/trypanosomiasis-human-african-(sleeping-sickness); 2018, Accessed on 03-02-2018.
12. Bowyer PW, Tate EW, Leatherbarrow RJ, Holder AA, Smith DF, Brown KA. N-myristoyltransferase: a prospective drug target for protozoan parasites. *Chem Med Chem.* 2008;3:402–408.
13. Caceres AJ, Michels PA, Hannaert V. Genetic validation of aldolase and glyceraldehyde-3-phosphate dehydrogenase as drug targets in Trypanosoma brucei. *Mol Biochem Parasitol.* 2010;169:50–54.
14. Merritt C, Silva LE, Tanner AL, Stuart K, Pollastri MP. Kinases as druggable targets in trypanosomatid protozoan parasites. *Chem Rev.* 2014;114:11280–11304.
15. Pizarro JC, Hills T, Senisterra G, et al. Exploring the Trypanosoma brucei Hsp83 potential as a target for structure guided drug design. *PLoS Negl Trop Dis.* 2013;7:e2492.
16. Oberholzer M, Marti G, Baresic M, Kunz S, Hemphill A, Seebeck T. The Trypanosoma brucei cAMP phosphodiesterases TbrPDEB1 and TbrPDEB2: flagellar enzymes that are essential for parasite virulence. *FASEB J.* 2007;21:720–731.
17. Bland ND, Wang C, Tallman C, et al. Pharmacological validation of Trypanosoma brucei phosphodiesterases B1 and B2 as druggable targets for African sleeping sickness. *J Med Chem.* 2011;54:8188–8194.
18. de Koning HP, Gould MK, Sterk GJ, et al. Pharmacological validation of Trypanosoma brucei phosphodiesterases as novel drug targets. *J Infect Dis.* 2012;206:229–237.
19. Orrling KM, Jansen C, Vu XL, et al. Catechol pyrazolinones as trypanocidals: fragment-based design, synthesis, and pharmacological evaluation of nanomolar inhibitors of trypanosomal phosphodiesterase B1. *J Med Chem.* 2012;55:8745–8756.
20. Boswell-Smith V, Spina D, Page CP. Phosphodiesterase inhibitors. *Br J Pharmacol.* 2006;147:S252–S257.
21. Seldon PM, Barnes PJ, Meja K, Giembycz MA. Suppression of lipopolysaccharide-induced tumor necrosis factor-alpha generation from human peripheral blood monocytes by inhibitors of phosphodiesterase 4: interaction with stimulants of adenylyl cyclase. *Mol Pharmacol.* 1995;48:747–757.
22. Souness JE, Rao S. Proposal for pharmacologically distinct conformers of PDE4 Cyclic AMP phosphodiesterases. *Cell Signal.* 1997;9:227–236.
23. Veerman J, van den Bergh T, Orrling KM, et al. Synthesis and evaluation of analogs of the phenylpyridazinone NPD-001 as potent trypanosomal TbrPDEB1 phosphodiesterase inhibitors and in vitro trypanocidals. *Biorg Med Chem.* 2016;24:1573–1581.
24. Amata E, Bland ND, Hoyt CT, Settimo L, Campbell RK, Pollastri MP. Repurposing human PDE4 inhibitors for neglected tropical diseases: design, synthesis and evaluation of cilomilast analogues as Trypanosoma brucei PDEB1 inhibitors. *Bioorg Med Chem Lett.* 2014;24:4084–4089.
25. Blaazer AR, Singh AK, de Heuvel E, et al. Targeting a subpocket in Trypanosoma brucei phosphodiesterase B1 (TbrPDEB1) enables the structure-based discovery of selective inhibitors with trypanocidal activity. *J Med Chem.* 2018.
26. Jansen C, Wang H, Kooistra AJ, et al. Discovery of novel trypanosoma brucei phosphodiesterase B1 inhibitors by virtual screening against the unliganded TbrPDEB1 crystal structure. *J Med Chem.* 2013;56:2087–2096.
27. De Heuvel E, Singh AK, Edink EE, et al. Alkynamide phthalazinones as a new class of TbrPDEB1 inhibitors, part 1. *Biorg Med Chem.* 2019 In press.
28. Korb O, Stützle T, Exner TE. Empirical scoring functions for advanced protein − ligand docking with PLANTS. *J Chem Inf Model.* 2009;49:84–96.
29. Marcou G, Rognan D. Optimizing fragment and scaffold docking by use of molecular interaction fingerprints. *J Chem Inf Model.* 2007;47:195–207.
30. Kooistra AJ, Vischer HF, McNaught-Flores D, Leurs R, de Esch IJP, de Graaf C. Function-specific virtual screening for GPCR ligands using a combined scoring method. *Sci Rep.* 2016;6:28288.
31. Ken-ichi O, Taichi S, Shan ZC, Isamu I. An efficient synthesis of β-aroylacrylic acid ethyl ester by the friedel-crafts reaction in the presence of diethyl sulfate. *Chem Lett.* 2006;35:22–23.
32. Huitric AC, Carr JB, Trager WF, Nist BJ. Configurational and conformational analysis: axial-axial and axial-equatorial coupling constants in six-membered ring compounds. *Tetrahedron.* 1963;19:2145–2151.
33. Oberholzer M, Saada EA, Hill KL. Cyclic AMP regulates social behavior in african trypanosomes. *mBio.* 2015;6.
34. Jansen C, Kooistra AJ, Kanev GK, Leurs R, de Esch IJP, de Graaf C. PDEStrIAn: a phosphodiesterase structure and ligand interaction annotated database as a tool for structure-based drug design. *J Med Chem.* 2016;59:7029–7065.
35. Winter G, Lobley CMC, Prince SM. Decision making in xia2. *Acta Crystallographica Section D.* 2013;69:1260–1273.
36. Vonrhein C, Flensburg C, Keller P, et al. Data processing and analysis with the autoPROC toolbox. *Acta Crystallographica Section D.* 2011;67:293–302.
37. Kabsch W. Integration, scaling, space-group assignment and post-refinement. *Acta Crystallographica Section D.* 2010;66:133–144.
38. Evans PR, Murshudov GN. How good are my data and what is the resolution? *Acta Crystallographica Section D.* 2013;69:1204–1214.
39. Battye TGG, Kontogiannis L, Johnson O, Powell HR, Leslie AGW. iMOSFLM: a new graphical interface for diffraction-image processing with MOSFLM. *Acta Crystallographica Section D.* 2011;67:271–281.
40. Winn MD, Ballard CC, Cowtan KD, et al. Overview of the CCP4 suite and current developments. *Acta Crystallographica Section D.* 2011;67:235–242.
41. McCoy AJ, Grosse-Kunstleve RW, Adams PD, Winn MD, Storoni LC, Read RJ. Phaser crystallographic software. *J Appl Crystallogr.* 2007;40:658–674.
42. Emsley P, Lohkamp B, Scott WG, Cowtan K. Features and development of Coot. *Acta Crystallographica Section D.* 2010;66:486–501.
43. Murshudov GN, Skubak P, Lebedev AA, et al. REFMAC5 for the refinement of macromolecular crystal structures. *Acta Crystallographica Section D.* 2011;67:355–367.
44. The PyMOL Molecular Graphics System, Version 1.7, Schrödinger, LLC.
45. Wirtz E, Leal S, Ochatt C, Cross GM. A tightly regulated inducible expression system

for conditional gene knock-outs and dominant-negative genetics in Trypanosoma brucei. *Mol Biochem Parasitol.* 1999;99:89–101.
46. Oberholzer M, Lopez MA, Ralston KS, Hill KL. Chapter 2 – Approaches for Functional Analysis of Flagellar Proteins in African Trypanosomes. In: King SM, Pazour GJ, eds. *Methods Cell Biol.* Academic Press; 2009:21–57.
47. Nikolaev VO, Bünemann M, Hein L, Hannawacker A, Lohse MJ. Novel single chain cAMP sensors for receptor-induced signal propagation. *J Biol Chem.* 2004;279:37215–37218.
48. Oberholzer M, Langousis G, Nguyen HT, et al. Independent analysis of the flagellum surface and matrix proteomes provides insight into flagellum signaling in mammalian-infectious *Trypanosoma brucei*. *Mole Cell Proteom: MCP.* 2011;10 M111.010538-M010111.010538.
49. Schlaeppi K, Deflorin J, Seebeck T. The major component of the paraflagellar rod of Trypanosoma brucei is a helical protein that is encoded by two identical, tandemly linked genes. *J Cell Biol.* 1989;109:1695–1709.